

Review

Catalyst-Doped Anodic TiO₂ Nanotubes: Binder-Free Electrodes for (Photo)Electrochemical Reactions

Hyeonseok Yoo ¹, Moonsu Kim ¹, Yong-Tae Kim ¹, Kiyoung Lee ^{2,*}  and Jinsub Choi ^{1,*} 

¹ Department of Chemistry and Chemical Engineering, Inha University, 100 Inha-ro, Nam-gu, Incheon 22212, Korea; hsyoo1124@inha.ac.kr (H.Y.); moonsk310@inha.edu (M.K.); philosaint84@gmail.com (Y.-T.K.)

² School of Nano and Materials Science and Engineering, Kyungpook National University, 2559 Gyeongsang-daero, Sangju, Gyeongbuk 37224, Korea

* Correspondence: kiyoung@knu.ac.kr (K.L.); jinsub@inha.ac.kr (J.C.); Tel.: +82-54-530-1333 (K.L.); +82-32-860-7460 (J.C.)

Received: 31 October 2018; Accepted: 13 November 2018; Published: 17 November 2018



Abstract: Nanotubes of the transition metal oxide, TiO₂, prepared by electrochemical anodization have been investigated and utilized in many fields because of their specific physical and chemical properties. However, the usage of bare anodic TiO₂ nanotubes in (photo)electrochemical reactions is limited by their higher charge transfer resistance and higher bandgaps than those of semiconductor or metal catalysts. In this review, we describe several techniques for doping TiO₂ nanotubes with suitable catalysts or active materials to overcome the insulating properties of TiO₂ and enhance its charge transfer reaction, and we suggest anodization parameters for the formation of TiO₂ nanotubes. We then focus on the (photo)electrochemistry and photocatalysis-related applications of catalyst-doped anodic TiO₂ nanotubes grown on Ti foil, including water electrolysis, photocatalysis, and solar cells. We also discuss key examples of the effects of doping and the resulting improvements in the efficiency of doped TiO₂ electrodes for the desired (photo)electrochemical reactions.

Keywords: TiO₂ nanotubes; anodization; doping; water electrolysis; photoanodes

1. Introduction

Anodization is a facile process that allows the physical and chemical properties of an entire metal surface to be modified at a very low cost, and it has long been recognized as a well-established industrial surface treatment technique [1,2]. In particular, the discovery of self-ordering phenomena in anodic aluminum oxide produced using two-step anodization [3–6] led to great advances in nanoscience applications based on highly ordered nanoporous Al₂O₃ membranes and triggered the search for new alternative anodic materials with intrinsic semiconductive properties induced by external electrical or photo stimuli [7].

One such material is anodic titanium oxide. Its morphology, and thus its chemical and physical properties, can be easily tuned by electrochemical anodization [8–11]. Unlike anodic aluminum oxide (>7.5 eV), anodic titanium oxide has a moderate bandgap (~3.1 eV), can form unique morphologies such as nanotubular, microconical, fishbone-like structures, and can be directly grown on a Ti substrate [9–14]. TiO₂ itself possesses photocatalytic properties and inherent resistance to corrosion under harsh environmental conditions [8,15,16].

Since the formed oxide adheres to and remains in stable contact with the mother metal material without any binder, high-surface-area anodic titanium oxide has been considered for use as an electrode for (photo)electrochemical reactions in strong acidic or basic conditions [17,18]. In general, electrodes should require a low overpotential for initiating the targeted reaction in order to increase current efficiency. However, oxide-based electrodes containing anodic titanium oxide are disadvantageous

in this regard, as their charge transfer resistance is higher than that of metal-based electrodes [19]. Thus, modification of the electrode material with catalysts has been used to enhance charge-transfer at the interface between the electrode and the electrolyte and to lower the overall overpotential of electrodes that are affordable to use in highly corrosive environments or environments requiring long-term stability. For example, electrodes that can effectively split water into hydrogen and oxygen by electrolysis have attracted attention for use in hydrogen generation, a key issue in sustainable energy generation and storage systems [20]. Due to the higher overpotential and sluggishness of the oxygen eVolution reaction (OER) in acidic media than that of the hydrogen eVolution reaction (HER), the OER is the rate-limiting step for the development of high-efficiency water electrolyzers [20–22]. Usually, noble metals are utilized as active catalysts, with Pt being commonly used for the cathode and Ir, Ru, or both being used for the anode. The HER in alkaline media is a more interesting reaction, as non-noble catalysts such as Co, Ni, and Fe work nearly as well as Ir or Ru catalysts [23]. In addition, high-surface-area TiO₂ nanotubes containing trace amounts of Ru or Ir catalysts have also been demonstrated to be applicable as OER electrodes in alkaline media [24].

In photo-electrochemistry or photo-catalysis-related applications, the bandgap and band positions are very important, as they determine the energy (or H₂) conversion efficiency from solar energy [15,25]. Because the inherent bandgap of TiO₂ falls in the UV region, TiO₂ nanotubes must be doped with foreign elements (N, S, P, Ru, Ta, Nb, WO₃, MoO₃, etc) to improve their photocatalytic properties. However, due to the high-aspect-ratio of nanotubes grown on a Ti substrate, uniform and homogenous doping (or decoration) of foreign elements in (or on) the entire surface of the nanotubes is very difficult to achieve.

Very recently, several technical advances for the doping of active materials into high-aspect-ratio TiO₂ nanotubes without causing structural damage have been reported by several groups [26–32]. For example, Ti alloys containing active catalysts were anodized under suitable anodization conditions to produce nanotubular anodic TiO₂ containing foreign catalysts [30]. The simplest method involves doping with N or C by annealing TiO₂ under a N- or C-providing environment [26–29]. In addition, anodization can be carried out in a F[−]-based electrolyte containing a negatively charged precursor (for example, RuO₄[−], which is dissociated from KRuO₄) that can be incorporated into the anodic oxide during the anodization, the growth of anodic TiO₂ nanotubes occurs and doping with the foreign catalyst occur simultaneously (so-called single-step anodization for doping). Alternatively, immediately after the fabrication of nanotubes, the F[−]-containing electrolyte, which is essential for the formation of nanotubes, can be replaced with an electrolyte containing the negatively charged precursors. Subsequently, a potential higher than that used for anodization is applied to the nanotubes in the precursor solution to dope the negatively charged ions into the oxide (potential shock for doping) [31–33].

Although each method has its advantages, both give rise to some issues during the doping process. Specifically, in single-step anodization, some precursors are self-reduced in the electrolyte by F[−] ions. For example, when single-step anodization is carried out using MnO₄[−] in an F[−]-based electrolyte, the Mn is deposited on the counter electrode in metallic form rather than being doped into TiO₂ as MnO₄[−] due to the facile reduction of MnO₄[−] to Mn²⁺ [34]. In the potential shock method, the barrier oxide on the bottom of nanotubes grows significantly thicker with increasing potential shock voltage, blocking current flow. Although higher potentials produce higher doping concentrations in the nanotubes, very high potential shock voltages cannot be used due to the barrier layer growth. Therefore, optimization of the potential shock voltage always involves a trade-off between achieving a high degree of doping and reducing the growth of the barrier oxide. Additionally, although electrolytes with high precursor concentrations result in higher doping concentrations in TiO₂, in some cases the target potential cannot be maintained due to the limiting current-compliance of the power supply [34]. Thus, low potential shock voltages and low concentrations of doping precursors are preferred in the potential shock method, meaning that relatively low doping concentrations are achieved. In general, Cl[−]-based ions destroy or break down nanotubular structures during simultaneous single-step anodization or

potential shock doping. However, some novel metal precursors inherently produce Cl^- ; for example, H_2PtCl_6 is dissociated to $2\text{H}^+ + \text{PtCl}_6^{2-}$, which generates Cl^- ions. In such cases, underpotential shock, in which the potential shock voltage is lower than that used for anodization, has been successfully demonstrated as an alternative doping method. In that case, the Pt ions penetrate only the middle of the oxide layer where the low potential shock voltage has an influence, rather than reaching the interface of the barrier oxide and the Ti metal [33].

The anodization of alloys is another method to produce doped TiO_2 nanotubes; however, the alloying process is very elaborate compared to the fabrication of Ti metal alone. Due to limit of availability of Ti-based alloys and their cost, a great deal of work to develop easily reproducible metal alloys at low cost is still required [30]. Additionally, the inevitable thermal growth of additional oxides and crystal phase changes as a function of the temperature during the annealing process should be considered [35].

Recently, a number of review or prospective articles related to anodic TiO_2 and its applications have been published. For example, Lee et al. comprehensively reviewed one-dimensional titanium oxides grown by anodization [8]. More specifically, several groups have published reviews of photo-catalysis or electro-catalysis applications based on anodic TiO_2 [36–40]. Additionally, bio-related applications of anodic TiO_2 materials have also been reviewed recently [41,42].

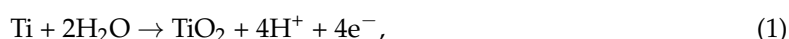
In this review, we focus on the use of TiO_2 nanotubes as (photo)electrochemical binder-free electrodes in applications that require low overpotential or narrow bandgaps to achieve the desired reactions. Various doping processes to adjust the overpotential and bandgap are comprehensively reviewed.

2. Formation Mechanisms of TiO_2 Nanotubes

2.1. Reaction Mechanism

The formation of TiO_2 nanotubes is governed by two competitive reactions: (1) oxide formation at the oxide/metal interface by oxygen anions (O_2^- and OH^-), and (2) the dissolution reaction caused by the F^- in the electrolyte (Figure 1) [2,8,10,11,16,36].

In oxide formation, O_2^- and OH^- anions evolve on the electrolyte/oxide interface via the electrolysis of water. These anions diffuse through the oxide layer to come into contact with the metal interface. Simultaneously, Ti^{4+} moves through the oxide layer in the opposite direction, and reacts directly with oxygen anions. Eventually, TiO_2 is generated as shown in the equation below [8,11,16,43].



In short, the oxide formation rate is governed by the diffusion and reaction rates of the oxygen anions in the oxide layer. The newly formed oxide pushes up the existing oxide and gradually grows toward the metal substrate. This phenomenon is known as “plastic flow” [11].

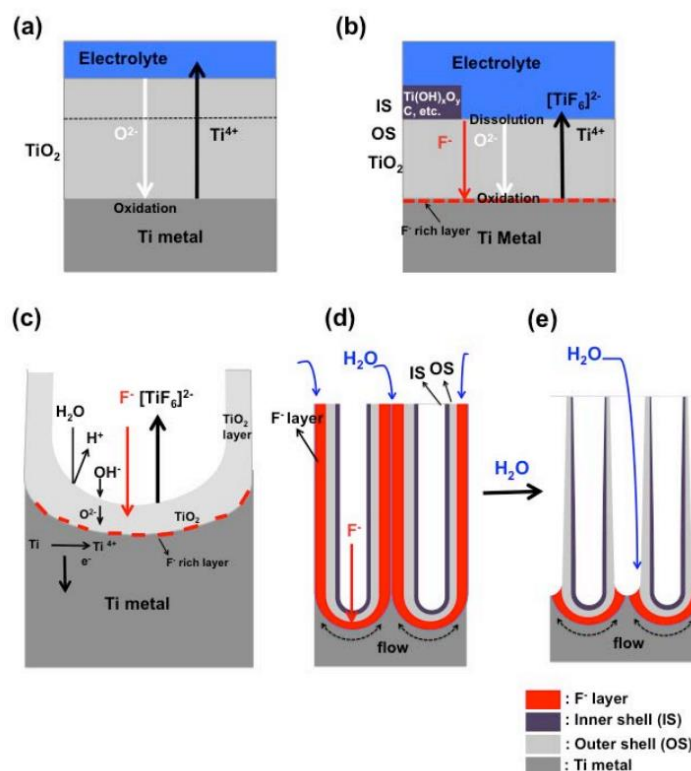


Figure 1. Schematic of the reaction mechanism of TiO_2 anodization. (a) O^{2-} and Ti^{4+} are transported through the oxide layers due to the electric field. (b) In presence of fluoride ions, $[\text{TiF}_6]^{2-}$ and an F^- -rich layer are generated. The initial formation of a tubular structure is shown in (c), and in (d) and (e) the F^- -rich layer is finally dissolved by the water in the electrolyte. Reproduced with permission from ref [11]. Friedrich-Alexander-Universität Erlangen-Nürnberg (2013).

Meanwhile, in the dissolution reaction, F^- ions react with TiO_2 directly at the electrolyte/oxide interface to produce $[\text{TiF}_6]^{2-}$, which is easily dissolved into the electrolyte due to its high solubility in water. As the F^- ions travel roughly twice as fast as the oxygen ions, they can contact and react directly with Ti^{4+} at the oxide/metal interface. The relevant reaction equations are follows [8,11,16]:



Due to the role of F^- , the honeycomb-like porous structure transforms into an array of tubes with an F^- -rich layer between the TiO_2 layer and the Ti metal. As a result, a hemispherical oxide/metal interfacial structure is formed. The overall growth rate and the length of the nanotubes are determined by the difference between the oxide formation and dissolution reaction rates.

The current–time (I-t) behavior measured during the potentiostatic preparation of TiO_2 nanotubes reflects this overall mechanism (Figure 2). In the initial stage, the current decreases rapidly due to the increasing resistance of the rapidly growing oxide layer (I). In the second step (II), the current increases slightly due to the formation of nano-sized pits, which are formed due to attack by the F^- ions. The local electric fields are strengthened in these pits, thus attracting more anions to participate in the oxide formation and dissolution reactions. As a tubular structure begins to form beneath the pits, the current decreases again (III). When the oxide formation and dissolution reactions reach equilibrium, the current converges (IV). The current–time transient itself cannot confirm the formation of nano-tubular structures, since non-nanotube-forming processes based on the barrier oxide formation, oxide pitting, and the stable growth mechanism show similar current patterns [11].

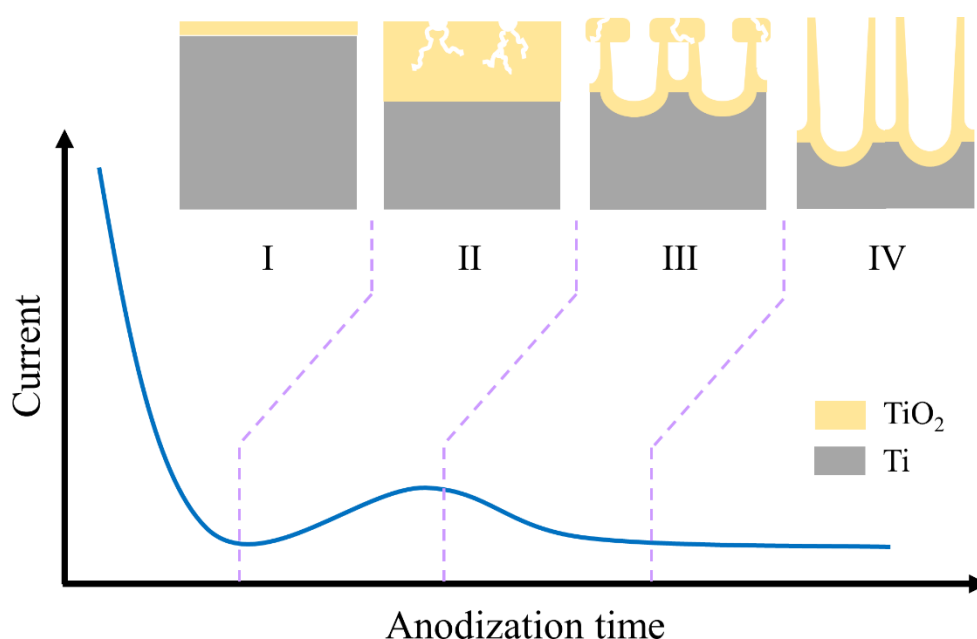


Figure 2. A representative current–time curve for the formation of tubular structures. (I) The current decreases drastically due to the growth of the barrier oxide during initial stage of anodization. Next, (II) nano-pits or cracks caused by F^- ions cause an increase in the current due to the concentrated electric fields on these pits. Once the tubular structure has formed and is growing evenly, the current declines and converges at a stable value due to the increased diffusion length of the ions involved in the reaction. Reproduced with permission from ref [11]. Friedrich-Alexander-Universität Erlangen-Nürnberg (2013).

2.2. Reaction Parameters

TiO_2 nanotubes can be obtained in electrolytes containing halides (ClO_4^- , Br^- , Cl^- , F^-), regardless of the electrolyte solvent. The use of F^- salts is favorable to prepare uniformly oriented TiO_2 nanotube arrays [31,44,45]. When Cl^- or Br^- are added to the electrolyte, non-uniform bundle-like nanotubular structures are easily generated; this is known as rapid breakdown anodization (RBA) [30,44–46]. Generally, 0.05–2% F^- ion is considered to be appropriate for the formation of TiO_2 nanotubes [11,31]. After selecting the F^- concentration, the environment of the electrolyte is determined depending on the type of solvent. HF is a typical F^- source that is widely utilized in aqueous conditions. Additionally, it is recommended to adjusting the pH of electrolyte to neutrality; sulfuric acid, phosphoric acid, and acetic acid are typical acids used for this purpose, and NaOH or KOH are generally used as bases. Shifting the pH of the solution into the weakly acidic range results in longer nanotubes [47–49]. Feasible anodization voltages range from 5 to 30 V in aqueous conditions [11].

Ethylene glycol and glycerol are the most commonly used organic solvents for TiO_2 nanotube growth. The use of ethylene glycol is favored due to the low glycerol solubility of F^- containing salts such as NH_4F , which are widely used as the F^- source [50,51]. When these solvents are used, the electrolyte is normally weakly basic, demonstrating that basic conditions can also be used to prepare TiO_2 nanotubes. However, water is an essential component for the generation of TiO_2 . For this reason, 1–10% of water is usually added directly to the organic electrolyte [8,11,16,31,43]. TiO_2 nanotubes can be prepared over a very wide range of applied voltages in ethylene glycol; they are easily and uniformly grown via potentiostatic methods without any additional control technique in the range 25–100 V [31,52]. The recently reported ramping method is a powerful solution to avoid the breakdown of the oxide and to form nanotubes evenly at voltages above 100 V under organic conditions [52,53].

The pore size of the TiO_2 nanotubes is governed by intensity of the applied voltage. Normally, pores with sizes of 10–100 nm can be produced using the typical voltage ranges given

above [11,44,54,55]. For instance, a pore size of around 100 nm is easily obtained at 20 V. Similarly, the size of the pores produced in ethylene glycol solution is proportional to the applied voltage, but a voltage of 40–45 V corresponds to a pore size of 100 nm [31,56,57].

Moreover, it has been reported that the pore size can be expanded to 600 nm or more using the ramping technique, similarly to in the anodization of aluminum [52,53].

If the oxide formation rate is faster than the oxide dissolution rate, the length of the TiO₂ nanotubes will increase as a function of anodization time. When the rates of these two competitive reactions are in a steady-state equilibrium, the growth of nanotubes is halted, and they maintain their length. In general, TiO₂ nanotubes prepared in an organic electrolyte are much longer than those prepared in aqueous solution. The longest reported nanotubes produced under aqueous conditions were of 7.3 μm in length, but 1–3 μm nanotubes are achieved in most cases [11,31,49,58,59]. In contrast, nanotubes tens or hundreds of μm in length can be grown in ethylene glycol, allowing researchers to adjust the length of the nanotubes from a few hundreds of nanometers to micrometers by controlling the anodization time [8,31,56,57]. However, longer anodization time causes the formation of nanograsses, which are produced by nanotubes splitting in the direction of the applied electric field of the F[−] ions. Since the nanoglass blocks the movement of ions into the pores, several methods for its removal have been developed [13,59].

3. Doping of TiO₂ Nanotubes

As mentioned earlier, TiO₂ nanotubes provide an enormous electrochemical reaction surface area due to their high aspect-ratio. For example, TiO₂ nanotubes with a pore diameter of 100 nm and the aspect-ratio of 10 provide a surface area that is 120 times higher (0.785 cm² → 94.2 cm²) than that of a flat TiO₂ surface [31]. Nonetheless, suitable catalysts or active materials must be used to overcome the insulating properties of TiO₂. In this section, we discuss methods of doping TiO₂ nanotubes.

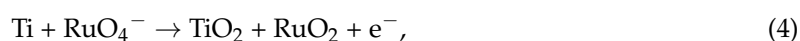
3.1. Electrochemical Doping Methods

3.1.1. Single-Step Anodization

Single-step anodization is a doping method based on the principle of plastic flow. The salt of an anion complex containing the target metal oxide is selected as the precursor. This salt is added directly to the conventional electrolyte to prepare the nanotubes. As shown in Figure 3a, nanotubes will not be produced if the electrolyte is not suitable for the typical anodic conditions used to produce nanotubular structures [17,24,31,47]. In addition, an electrolyte is difficult to be used if the precursor is vulnerable to F[−] ion [34].

The doping mechanism is almost the same as the anodization mechanism. The precursor anion participates in the two main reaction processes of oxide formation and dissolution. If the target dopant is Ru or Ir oxide, which are widely used for water oxidation catalysts, the catalyst doped into the nanotubes can be partially dissolved via the oxygen evolution reaction during prolonged anodization [17,24,31]. As a result, the doping concentration of the catalyst at the growth site will be much higher than that of the sidewalls of the nanotubes (Figure 3b).

Yoo et al. successfully doped RuO₂ into TiO₂ nanotubes via single-step anodization in an ethylene-glycol-based electrolyte containing 0.25% NH₄F and 5% water. RuO₂-doped TiO₂ nanotubes with a doping concentration of 0.12 at.% were produced in the same anodizing electrolyte with the addition of 0.02 M KRuO₄. The RuO₂-doped TiO₂ nanotubes prepared at 40 V for 22 h were approximately 30% longer than conventional nanotubes prepared without KRuO₄ [17]. The doping concentration increased to 1.21 at.% when an aqueous medium was used due to the effect of water. During the synthesis of the nanotubes, the precursor KRuO₄ is dissociated into K⁺ and RuO₄[−], the latter of which takes part in the following relevant reactions:



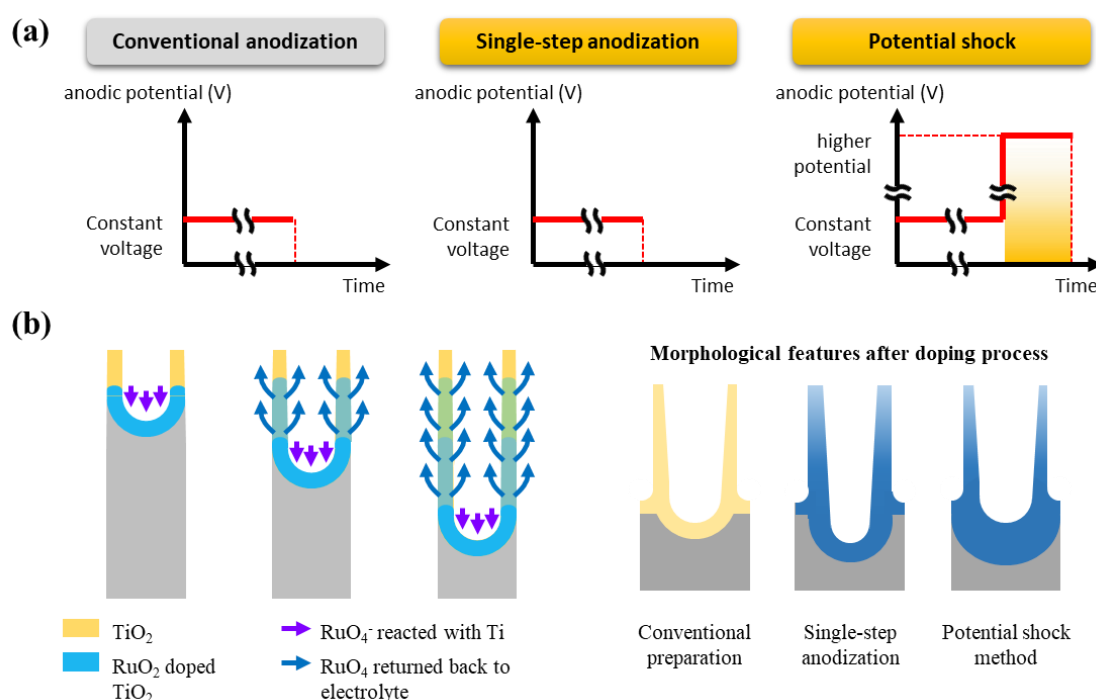
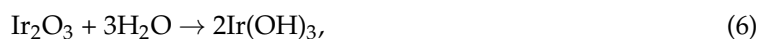


Figure 3. (a) A schematic of the conventional anodization procedure and doping methods. Note that potential shock is a sequential two-step anodic process. (b) Left: The doping of the catalysts follows “plastic flow.” The doped catalysts are able to partially dissolve at long doping times, as the high anodic potential induces the oxygen evolution reaction. Right: The morphologies of the doped TiO₂ nanotubes depends on the doping method. Reproduced with permission from ref [31]. Inha University (2018).

As shown in Equations (4) and (5), both RuO₂ and TiO₂ are formed from RuO₄⁻ simultaneously. As a result, the wall thickness of the nanotubes increased, as shown in Figure 4. The wall thickness of the nanotubes increases from 5.73 nm to 13.96 nm in the presence of the catalyst precursor of K₂RuO₄. The thickness can be further increased (13.96 nm → 25.74 nm) when electrolyte contains small amount of water, which can be explained by simultaneous formation of TiO₂ and RuO₂ in Equations (4) and (5). The rutile RuO₂ phase determined by SAED analysis provides a clear evidence for doping (Figure 4d).

Furthermore, simultaneous co-doping of TiO₂ nanotubes with IrO₂ and RuO₂ can be achieved by single-step anodization using the electrolyte 1 M H₃PO₄ + 1 M NaOH + 0.3–0.7 vol.% HF containing K₂RuO₄ and IrO_x nanoparticles, which are prepared as an intermediate species for IrO₂ doping. Since chloride ions, which damage the NTs, are typically involved in Ir precursors, IrO_x nanoparticles are used to generate IrO₄⁻ in the electrolyte along with the RuO₄⁻ for RuO₂ doping [24].



Therefore, the overall morphology of co-doped TiO₂ is similar to that of TiO₂ nanotubes singly doped with RuO₂. Under the optimized conditions, the doping concentration of IrO₂ in the TiO₂ layer of binary-catalyst-doped TiO₂ is usually about half that of RuO₂, exhibiting polycrystalline after annealing.

Tin oxide is also frequently used as a dopant to control the bandgap and overpotential of TiO₂. Unlike the doping precursors discussed above, tin oxide, which can be easily obtained from Na₂SnO₃, is used at basic pH; basic conditions are not typically used for the anodization of Ti in aqueous conditions. Ma et al. reported that an ethylene glycol-based electrolyte containing both Na₂SnO₃ and Na₂MoO₄·4H₂O led to the formation of TiO₂ nanotubes containing both 0.28% MoO₃ (Mo⁶⁺) and 0.51 at.% SnO₂ (Sn⁴⁺) [60].

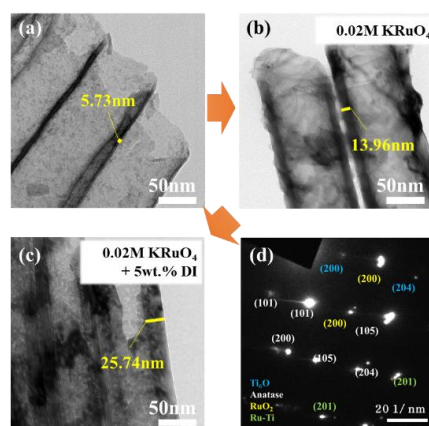


Figure 4. (a) TiO₂ nanotubes grown conventionally in ethylene glycol. (b) The thickness of the TiO₂ nanotubes is almost doubled by adding RuO₄[−] (as KRuO₄) to the electrolyte during single-step anodization. (c) The thickness of the TiO₂ nanotubes doped with RuO₂ is further increased by the addition of water to the RuO₂ precursor-containing electrolyte. (d) After doping via single-step anodization, a RuO₂ rutile phase is clearly observed in the TiO₂ anatase phase. Reproduced with permission from ref [17]. WILEY-VCH Verlag GmbH and Co. KGaA, Weinheim (2015).

Very recently, we reported that WO₃ can also be doped onto TiO₂ nanotubes using a phosphoric-acid-based aqueous electrolyte containing Na₂WO₄. The doping concentration increased linearly with the concentration of the precursor. The WO₃-doped TiO₂ nanotubes showed 17% higher electrochromic performance than bare TiO₂ nanotubes at the optimum doping concentration of 0.21 at.% [47].

3.1.2. Anodic Potential Shock

The anodic potential shock method was first reported by Jo et al. in 2009 [61]. Originally, it was designed for the preparation of through-hole type TiO₂ membranes. The same group later adopted this method to introduce dopants in/on anodic structures through modification of the anodization parameters [32,62,63]. This method is regarded as a two-step anodization, with each step being performed in a different electrolyte. In the first step, the formation of nanotubes takes place. In the second step, an extremely high anodic voltage is applied to the prepared nanotubes for a very short period (Figure 1a); the doping precursor is only present in the electrolyte used during the second step. The precursors used are almost the same as those in the single-step anodization, but the oxide formation and doping reactions are independent. Therefore, the oxide formation follows the anodization mechanism exactly (see Figure 1b), and the doping results from high-field migration under a sudden high potential.

We showed that RuO₂ could be doped into TiO₂ barrier structure via the potential shock method using KRuO₄ as the precursor [63]. The average doping concentration of Ru in TiO₂ at a shock voltage of 140 V was over 4 at.%. The two-step anodic doping method resulted in a much higher Ru concentration at the base of the nanotubes than in the walls, similarly to in single-step anodization [31,32]. However, additional barrier oxide was formed at the bottom of the tubes due to the absence of F[−] ions in the doping electrolyte; its thickness was a function of the applied potential shock voltage (see Figure 5). Using a similar method, Seong et al. succeeded in producing TiO₂ nanotubes with 0.7 at.% MnO₂

from the precursor KMnO_4 in ethylene glycol media; the nanotubes showed enhanced water oxidation performance under alkaline conditions [34].

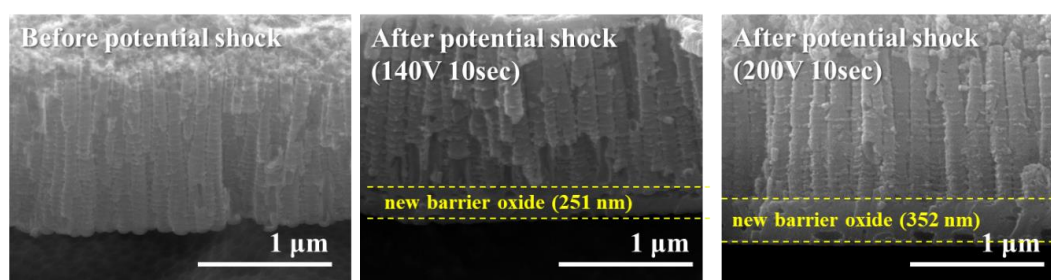


Figure 5. Cross-sectional scanning electron microscopy (SEM) images of RuO_2 -doped TiO_2 nanotubes prepared by the potential shock method. At the bottom of the tubes, additional barrier oxide was formed; the thickness of the barrier oxide depended on the applied shock voltage.

For Pt doping, Cl^- -based complexes such as H_2PtCl_6 are typically available as reaction-grade chemicals. Kim et al. prepared TiO_2 nanotubes doped with 3 ppm of PtO for application in the hydrogen eVolution reaction. In this case, a shock voltage below 20 V was utilized because higher voltages (over 20 V) caused the collapse of the tubular arrays via attack by the Cl^- ions. Since the applied potential shock voltage was far lower than the anodization voltage, this method is referred to as the underpotential shock method [33].

It is possible to use the potential shock method with any metal oxide catalyst, as long as the precursor is sufficiently soluble in a suitable solvent. However, the entrances to the pores must remain clear to allow the precursors easy access to the deep sites of the nanotubes. For this reason, TiO_2 nanotubes prepared in aqueous solution are much preferred. However, the possibility of using potential shock under other conditions has been suggested, as techniques to remove the nanograss that gradually develops during anodization have been reported [64–66].

3.2. Doping via Thermal Treatment

Anodically formed TiO_2 nanotube layers are normally amorphous [67,68]; however, when anodization is carried under specific conditions at higher voltages, nanocrystallites are present [35,67,69]. However, for use in many applications, the amorphous tubes must be crystallized by thermal treatment. In general, amorphous nanotubes can be converted to the anatase or rutile phases by thermal treatment at 300–500 °C or 550 °C, respectively. The bandgap energy of a crystallized TiO_2 nanotube is 3.2 eV after conversion to anatase, and 3.0 eV after conversion to rutile [68]. For certain applications, such as solar cells and photocatalysis, the bandgap energy of these structures is too wide. To enhance their efficiency in such applications, the bandgap energy must be tuned. The most well-known approach for adjusting the bandgap is to dope metal or non-metal impurities into the TiO_2 nanotubes.

Asahi et al. reported that nitrogen-doping of TiO_2 enhanced its visible photoresponse. Their report demonstrated that the doped nitrogen, which substituted for the oxygen of TiO_2 , narrowed the bandgap energy by introducing $\text{N}2\text{p}$ states just above the valence band of TiO_2 [15]. The classic approach to oxygen-substitution-doping of TiO_2 nanotubes involves ion implantation [26,27,70–72]. This method is most effective at introducing nitrogen into the TiO_2 lattice at low-to-medium doping levels (about 10^{18} ions/ cm^2) [26,27]. However, this method has several shortcomings: the ion penetration depth is limited to a few micrometers, a relatively high acceleration energy of several MeV is required, and the distribution of the dopant in the TiO_2 structure is often inhomogeneous. Moreover, after implantation, amorphization of the TiO_2 nanotubes occurs, making a reannealing process to reestablish the crystalline structure necessary. A simpler approach for doping nitrogen into TiO_2 is thermal treatment in NH_3 [70]. Such thermal treatments are generally performed in a NH_3/Ar atmosphere at relatively high temperatures (above 500 °C) [29].

Based on the peak position of nitrogen observed from sputtering TiO₂ under nitrogen atmosphere and titanium nitride [29], successful nitrogen doping should result in a nitrogen (N1s) peak located at ~396 eV in XPS analysis [28,29,72]. However, in some reports, this nitrogen peak was observed at ~400 eV or above 400 eV [73–75]. These higher peak values correspond to surface adsorption or sensitization of nitrogen on the TiO₂ surface as N–C compounds or molecular N₂ [76]. Several research groups have claimed to have successfully doped nitrogen into TiO₂ via solution-based doping. Other reports even claim that the nitrogen doping concentration in TiO₂ is increased by prolonged anodization. However, these results require further confirmation, as they resulted in N peaks located at ~400 eV [73–76]. Moreover, most of these reports did not show suitable evidence of bandgap engineering via visible photocurrent spectra or visible photocatalytic activity.

Carbon has also been suggested as a dopant to form states near the valence band by the substitution of oxygen [25,77,78]. Furthermore, carbon doping can also be achieved by the thermal treatment of TiO₂ in a carbonaceous environment or ashing organic compounds, such as CO or acetylene [79–81]. The thermal doping of carbon should be carefully defined to differentiate it from graphitization or the formation of oxy-carbides of the TiO₂ nanotubes [82,83]. The thermal treatment of TiO₂ nanotubes in an acetylene environment can also convert them to TiO_xC_y materials with semimetallic conductivity comparable to that of graphite [83]. Solution-based carbon doping is also frequently attempted. However, these results cannot consider carbon residue from decomposition of the organic electrolyte. The organic solvent in the anodization electrolyte can be decomposed by the applied high potential and remain inside the nanotube wall [67,84].

3.3. Alloy-Based Anodization

The simplest and most straightforward doping approach is the anodization of alloys that contain the dopant material. Using this method, nitrogen-doped TiO₂ nanotubes can be obtained by the anodization of TiN substrates [85,86], which can be prepared by arc-melting Ti and TiN powders. A similar approach involves anodizing Ti-transition metal alloys to produce metal- or metal-oxide-doped TiO₂ nanotubes [87–89]. Density functional theory (DFT) calculations have shown that various transition metals are effective dopants for Ti substitution in TiO₂ structures to form intermediate states in the bandgap [90]. The substitution of Ti by such dopants leads to a red-shift in the optical properties of the nanotubes [91–94], enhancing its electrical conductivity [95–98]. Metal oxides can also substitute Ti, as in the example of W doping. When tungsten is doped at Ti sites, it forms WO₃ in the TiO₂ lattice. Each W⁶⁺ associates with an extra oxygen instead of Ti⁴⁺. The WO₃-doped TiO₂ has a narrower bandgap as a result of its lower conduction band [99].

When preparing metal- or metal-oxide-doped TiO₂ nanotubes by the anodization of a Ti alloy, the dopant materials must not interfere with the anodic reaction. That is, in order to successfully prepare porous or tubular structures, only a very small amount of the dopant materials should be present in the Ti alloy, and the dopant materials should have chemical properties similar to those of Ti. If the chemical properties of the dopant are too different from those of Ti, or if too much dopant is present in the Ti alloy, the resulting nanotube structures may be irregular, or in the worst case, only a compact oxide will be formed (Figure 6).

In many cases, interesting morphology such as two-scaled nanotube structures (two length scales or two distinct tube diameters) are formed during the anodization of certain alloys [100–104]. Such morphologies may be caused by the different oxidation or dissolution kinetics of Ti and the dopant metals, but the phenomena are still not completely understood [105–107]. The metal composition of the anodic oxide formed from a Ti alloy depends on the metal ratio in the alloy substrate [108]. In some cases, small amounts of mixed oxides may be present in the anodic oxide structures. So far, complete mixed oxide conversion has only been reported for TiZr alloys [109].

Earlier studies of doped TiO₂ nanotubes prepared by the anodization of alloys focused on enhancing ion insertion to improve their electrochromic properties [87–89,110,111]. In particular, WO₃, MO₃, and Nb₂O₅-doped TiO₂ nanotubes formed by the anodization of Ti-W, Ti-Mo, and Ti-Nb alloys

showed significantly improved electrochromic efficiency and ion (particularly, H^+) insertion properties when even a small amount of dopant (0.2 at.% of WO_3) was present [87,88,110–113]. Moreover, $TiO_2-Nb_2O_5$ mixed-oxide nanotubes showed high ion intercalation stability and electrochromic activity. These results were due to the widening of the TiO_2 lattice by Nb ions, which was observed using high-resolution transmission electron microscopy (HRTEM) analysis and predicted by DFT calculations [88]. The lattice-widened TiO_2 nanotubes allow larger guest ions such as Li^+ and Na^+ to intercalate into the lattice, as well as making the H^+ intercalation process faster [88].

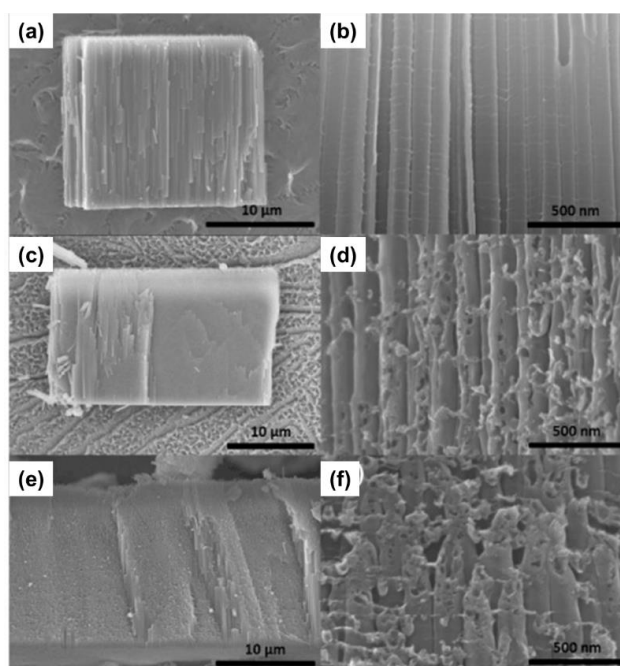


Figure 6. Representative cross-sectional SEM images of (a,b) regular and (c–f) irregular nanotubes formed by the anodization of Ti alloys. The nanotubes were formed by the anodization of Ti alloys containing (a,b) 0.02 at.%, (c,d) 0.05 at.%, and (e,f) 0.2 at.% of Ru. Reproduced with permission from reference [114]. WILEY-VCH Verlag GmbH and Co. KGaA, Weinheim (2012).

Obviously, the anodic oxidation of Ti alloys in F^- -containing electrolytes allows a wide range of dopants to be effectively doped into TiO_2 nanotubes. Moreover, the doped TiO_2 nanotubes formed from Ti alloys provide virtually unlimited potential to enhance the chemical and physical properties of the TiO_2 nanotubes. Specific examples of such enhancements will be discussed in the applications section.

4. Applications

4.1. Electrochemical Water Electrolysis

The electrochemical oxygen evolution reaction (OER) is a four-electron transfer reaction consisting of four single electron transfer reactions. Therefore, the use of catalysts is essential to reduce the overpotential, which is driven by the multiple electron transfer steps [115–117]. Increasing the amount of oxygen evolution at a given overpotential is becoming an important research topic [115,118]. A high reaction surface area is an important factor in producing a large amount of oxygen gas. Moreover, a durable support material is required, because the electrode is continuously exposed to corrosive oxygen radicals [119,120]. Thus, TiO_2 nanotubes, which have inherent anti-corrosive properties, are expected to be a good electrode material for this application. Decorating or doping catalysts onto/into high-aspect-ratio TiO_2 nanotubes is difficult, as the mouths of nanotubes can become blocked by precipitated catalyst if improper methods are employed. However, the problem of pore loss can be effectively solved by preparing the catalyst-assisted TiO_2 via the doping methods described in the previous sections.

TiO₂ nanotubes that are singly doped with RuO₂ via single-step anodization exhibit overpotentials in the range of 770–1000 mV [17,31,32,121]. The ideal Tafel plot slopes for the first, second, and third electron transfer steps in the OER mechanism have been reported to be 120, 40, and 30 mV/dec, meaning that the slope of Tafel should be lower than these values to achieve an excellent electron transfer rate. The Tafel slopes of nanotubes produced by single-step anodization are in the range of 37–46 mV/dec, indicating that the rate-determining step (RDS) for the OER in the nanotubes is located near the second electron transfer step. Nanotubes doped with RuO₂ using the potential shock method exhibit a lower overpotential (650 mV) than those produced via single-step anodization. However, the RDS when using these nanotubes for the OER has been reported to be the second electron transfer step, as they have a Tafel slope of 46 mV/dec [31,122–124].

The slow electron transfer of electrodes produced via the potential shock method can be explained in terms of morphological changes; the increased thickness of the barrier oxide at the bottom of the tubes increases the electron transfer resistance [31,54]. However, despite the thick barrier oxide, the overpotential of nanotubes prepared by the potential shock is lower than that of those prepared by single-step anodization. This is due to the surface chemical composition of the catalysts. Ru-O bonding, which effectively diminishes the overpotential, is dominant on the surface of the potential shock nanotubes [125–127]. On the other hand, Ru-OH, which increases the overpotential, is dominant on the surface of the single-step anodization nanotubes [31,121].

A complex variety of factors determine the current density in the OER. Increased surface area and an increased doping concentration of Ru in TiO₂ lead to higher current density, whereas increased barrier layer thickness reduces the current density (Figure 7). Overall, based on empirical experimental data from RuO₂-doped TiO₂ nanotubes, we found that the OER current is determined by three major factors according to the following relationship:

$$i \propto e^{(-\eta)} \frac{S \times C_{Ru}^2}{B^{1.5}} \quad (11)$$

i = end current density of LSV for OER

η = overpotential (0.1 M KOH vs. RHE)

C_{Ru} = average concentration of Ru determined by TEM EDS

S = calculated reaction surface area of electrode

B = average thickness of barrier oxide

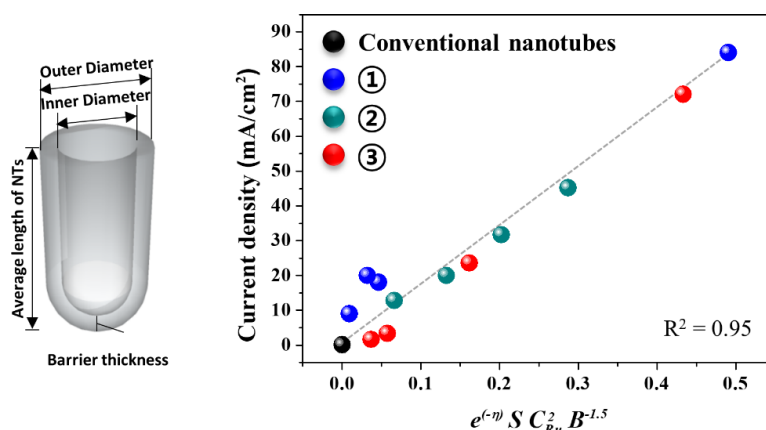


Figure 7. Linear relationship of the alkaline OER current density with the overpotential and the morphological parameters of doping concentration, surface area, and nanotube thickness for RuO₂-doped TiO₂ nanotubes. ①, ②, and ③ correspond to RuO₂ doping via single-step anodization in organic solvent, single-step anodization in aqueous conditions, and potential shock in aqueous conditions. Reproduced with permission from reference [31]. Inha University (2018).

TiO₂ nanotubes doped with MnO₂ via potential shock have been used as an improved non-noble metal catalyst in alkaline OER electrodes [34]. Pt, specifically PtO, which is doped into TiO₂ nanotubes by underpotential shock, provides enhanced performance in both the OER and HER (hydrogen eVolution reaction) [33]. RuO₂ and IrO₂ co-doping of TiO₂ nanotubes shows a synergetic effect in reducing overpotential. Such co-doped nanotubes exhibited an overpotential of 590 mV with the third electron transfer step [128]. This electrode eVolved twice the amount of oxygen gas compared to a powder-type electrode material with identical components (Figure 8) [24,128,129].

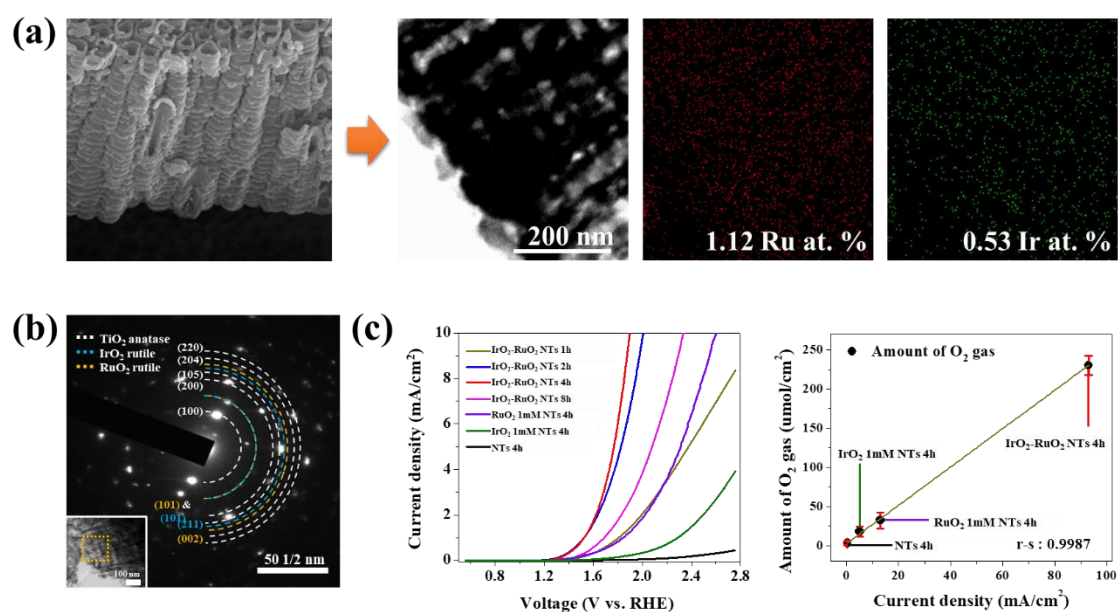


Figure 8. Morphological characterization data of IrO₂-RuO₂-doped TiO₂ nanotubes and the corresponding OER performance results. The elements (a) Ru (red spot) and Ir (green spot) are evenly distributed throughout the TiO₂. (b) The nanotubes are polycrystalline, with the rutile phase of RuO₂ and IrO₂ well-dispersed in TiO₂ anatase phase. (c) LSV graphs showing overpotentials and gas chromatography mass spectroscopy (GC-MS) results measured for different nanotube materials in identical alkaline OER tests. Reproduced with permission from reference [31]. Inha University (2018).

4.2. Photoanodes

4.2.1. Photocatalysis and Photoelectrochemical Water Splitting

Since the first report of photocatalytic water splitting on TiO₂ by Fujishima and Honda in 1972 [130], TiO₂ has been considered to be one of the best materials for photocatalysts. It has excellent photooxidative activity for the degradation of organic pollutants, toxins, and bacteria [130–136]. Two main reactions occur simultaneously in a photocatalytic system: photooxidation from holes on the surface of the valence band edge and photoreduction from the electrons on the surface of conduction band edge.

Enormous efforts have been dedicated to the study of the physical, chemical, and material properties of TiO₂ photocatalysts in order to enhance their activity. Recently, several investigations reported that anodic TiO₂ nanotube layers are more promising than nanoparticle layers for improving photocatalytic efficiency due to their well-defined geometry [67,79,137–146] and the ability to easily incorporate catalysts and dopants [141,147–151].

Among the various metal- and metal-oxide-doped TiO₂ nanotubes, WO₃-doped TiO₂ nanotubes most effectively increase photocatalytic activity [141]. In contrast to Al-doped nanotubes (one of the most efficient additives for inducing carrier recombination [89,141]), mixed-oxide TiO₂ nanotubes doped with both WO₃ and MoO₃ show strongly enhanced photocatalytic activity compared with non-doped tubes. The highly beneficial effect of W and Mo cannot be explained by better charge

transport in the tubes but is instead ascribed to modification of the band or surface state distribution of the doped nanotubes [89,112,141].

Photoelectrochemical water splitting is another promising application for anodic TiO₂ nanotubes. Like photocatalysis, the photoelectrochemical water splitting reaction is based on the light-induced electron–hole pair creation [140]. H₂O can be oxidized by the hole generated on the TiO₂ surface, and hydrogen eVolution occurs at the counter electrode (such as Pt) by attracting an electron from the TiO₂ conduction band. In this context, the electronic properties of TiO₂ are very important, because they determine how efficiently electrons can be transferred along the one-directional path. Hence, a wide range of investigations into the electrical and optical properties of TiO₂ nanotubes have been performed, as described above.

For photoelectrochemical water splitting, very low amounts of metal or metal oxide dopants such as RuO₂ [149], Nb [148,150], and Ta [151] are used. In RuO₂-doped TiO₂ nanotubes, the RuO₂ is believed to accelerate the O₂ eVolution reaction by catalytic activity [152–154]. On the other hand, TiO₂ nanotubes doped with small amounts of transition metal (such as Nb or Ta) show enhanced the electrical conductivity due to their narrower bandgaps, meaning that the electrons can travel efficiently through the TiO₂ layers to the back contact. The long electron lifetime significantly increases the water splitting efficiency [148,151].

4.2.2. Solar Cells

Another highly promising application of TiO₂ nanotubes is energy conversion devices such as dye-sensitized solar cells (DSSCs). In 1991, Grätzel and O'Regan reported the most significant achievement in this field, the first report of fully fabricated solar cell devices (DSSCs) [155]. The solar cells consisted of a nanocrystalline mesoporous TiO₂ thin-film electrode, a Ru–bipyridyl complex, and an iodine redox electrolyte, and showed a conversion efficiency of 11% [156,157].

As illustrated in Figure 9, electrons are excited from the highest occupied molecular orbital (HOMO) to the lowest unoccupied molecular orbital (LUMO) of the sensitized dye on the TiO₂ surface. The excited electrons are injected into the conduction band of the metal oxide on a femto- to picosecond timescale, and the oxidized dye molecules are reduced by the electrolyte redox reaction within nanoseconds. However, the electron transport rate in TiO₂ and the diffusion rate of the electrolyte are quite slow (micro- to milliseconds) (Figure 9a). For this reason, the overall cell efficiency is determined by the electron transport rate and electrolyte diffusion rate [158]. The electron transport rate and electrolyte diffusion rate compete with the recombination rate of the electrons. Generally, the electron transport rate in TiO₂ nanoparticles is considered to be relatively slow due to surface states, defects, and grain boundaries, which act as electron trapping sites and recombination sites [159–163].

In order to overcome the drawbacks of TiO₂ nanoparticles, one-dimensional TiO₂ nanostructures such as nanorods, nanowires, and nanotubes have been considered for use as photoanodes for DSSCs. Among these nanostructures, anodically formed TiO₂ nanotubes have been considered to be one of the most promising approaches to achieve vertically oriented nanostructures that lead to fast electron pathways [164–167]. However, the overall conversion efficiency of solar cells based on TiO₂ nanotubes is far lower than that of those based on classical nanoparticles. Anodic TiO₂ nanotube structures still have considerable room for improvement. Several approaches to enhance the overall conversion efficiency of DSSCs by modifying the nanotube structures have been considered. For example, the charge collection efficiency of nanotubes can be improved by electronic, surface, or geometric modification, which directly affects the amount of dye absorption. In addition, front-side illuminated cell construction obviously enhances light harvesting.

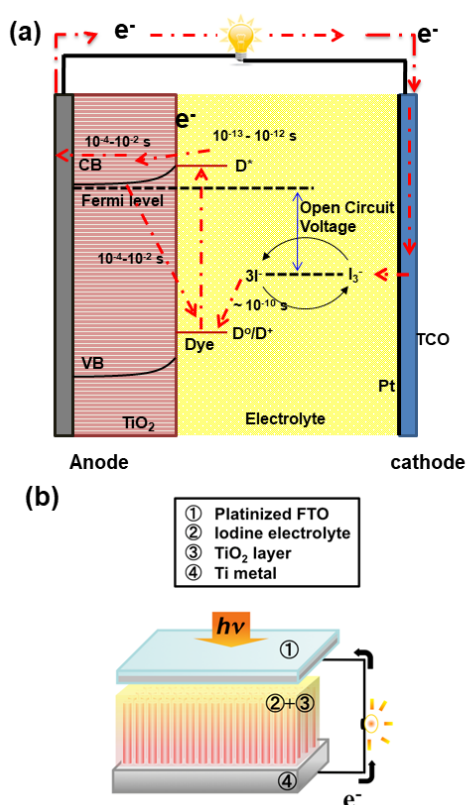


Figure 9. Schematic diagram of a dye-sensitized solar cell (DSSC): (a) Principle of a dye-sensitized solar cell and the time scales of various processes; (b) a full cell constructed with anodic TiO₂ nanotubes. Reproduced with permission from reference [8]. American Chemical Society (2014).

Metal (such as Nb, Ta or Ru) doping enhances the electrical conductivity of TiO₂ nanotubes for use in DSSCs [114,168,169]. Doped TiO₂ nanotubes have a slower recombination rate than bare TiO₂ nanotubes, improving the electron lifetime [114,168,169]. This beneficial effect has been demonstrated using intensity modulated photovoltage spectroscopy (IMVS), photocurrent spectroscopy (IMPS) measurements, and classical electrochemical impedance spectroscopy [114,168,169] (Figure 10). As a result, the overall conversion efficiency of doped TiO₂ nanotubes can be increased by 15–35% compared to non-doped TiO₂ nanotubes [114,168,169]. Interestingly, these positive effects vanish in nanostructures with high concentrations of the metal dopants.

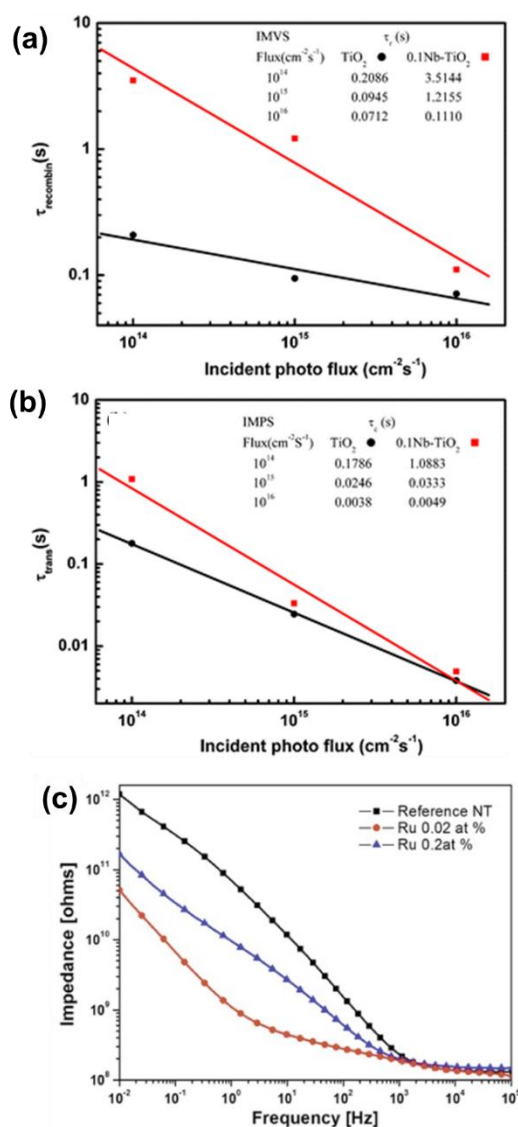


Figure 10. (a) Recombination time (τ_r) and (b) electron transfer (τ_c) constants calculated from IMVS and IMPS measurements for pure TiO₂ and 0.1 Nb–TiO₂ nanotube-layer-based DSSCs. (c) Electrochemical impedance measurements of TiO₂ and Ru-doped TiO₂ nanotubes in 0.1 M Na₂SO₄. Reproduced with permission from ref [168]. Royal Society of Chemistry (2010) and reference [114]. WILEY-VCH Verlag GmbH and Co. KGaA, Weinheim (2012).

5. Summary

This paper reviewed the growth of catalyst-doped anodic TiO₂ nanotubes and their applications as binder-free electrodes for highly desirable (photo)electrochemical reactions that require a low overvoltage or bandgap. A broad overview of techniques for doping the target materials into anodic TiO₂ nanotubes is given.

Concerning the growth of anodic TiO₂ nanotubes, we addressed the mechanisms of the reactions that occur during the anodization process and the reaction parameters that influence the structural morphologies of the tubes. The formation of anodic TiO₂ nanotubes is guided by oxide formation and dissolution at the interface between the oxide and metal substrate based on a “plastic flow model”. In general, electrolytes containing halide ions are suitable for the preparation of TiO₂ nanotubes; in particular, electrolytes containing 0.02–2% F[−] ions are widely used with a constant voltage of 5–30 V in aqueous conditions or 25–100 V in organic conditions.

Several techniques for doping foreign elements into high-aspect-ratio TiO₂ nanotubes to improve their catalytic properties have also been reviewed in detail. In single-step anodization, a salt of the anion complex containing the target metal oxide is used as the doping precursor, and is added directly to the electrolyte used for the formation of TiO₂ nanotubes under conventional voltage conditions. As the negatively charged precursor is incorporated into the anodic oxide during anodization, the growth of TiO₂ nanotubes and doping with the target element occur simultaneously. In the anodic potential shock method, the formation of the TiO₂ nanotubes and doping with the target element are performed independently in different electrolytes. After the TiO₂ nanotubes are fabricated, the electrolyte is replaced with an electrolyte containing the anion complex precursor and a potential higher than that of first anodization potential is applied for a short time, which leads to the doping of the negatively charged materials into the anodic oxide.

In addition to electrochemical doping methods, simple and straightforward doping approaches, such as the thermal annealing of TiO₂ nanotubes under a suitable environment or the anodization of an alloy containing the dopant materials can be employed.

Catalyst-doped anodic TiO₂ nanotubes lead to low overpotentials, which are favorable for initiating reactions. For this reason, they are considered to be promising electrodes for electrochemical applications. The overpotential for electrochemical water electrolysis can be reduced to 650 mV via doping of TiO₂ nanotubes. Due to the morphological changes and surface composition of the catalyst on the electrode surface, it is difficult to further reduce the overvoltage for OER.

In addition, metal or metal oxide (Nb, Ta, Ru, WO₃ or MoO₃)-doped TiO₂ nanotubes show superior photocatalytic and photoelectrochemical water splitting performance compared to non-doped TiO₂ nanotubes due to bandgap engineering and their surface state distribution. Nb, Ta, or Ru-doped TiO₂ nanotubes show higher overall conversion efficiency in DSSCs as a result of their slower recombination rate and enhanced electron lifetime.

Author Contributions: Supervision: K.L. and J.C.; Writing—original draft preparation: H.Y., K.L., M.K., Y.-T.K. and J.C.; Writing—review and editing, H.Y., K.L., M.K., Y.-T.K., and J.C.

Funding: This research was supported in part by the Basic Science Research Program through the National Research Foundation of Korea (NRF) funded by the Ministry of Education (NRF-2018R1A6A1A03024962), and in partly funded through the Human Resources Development program (Grant No. 20174030201500) of the Korea Institute of Energy Technology eValuation and Planning (KETEP) by the Ministry of Trade, Industry and Energy of the Korean government.

Conflicts of Interest: The authors declare no conflict of interest.

References

1. Keller, F.; Hunter, M.; Robinson, D.L. Structural features of oxide coatings on aluminum. *J. Electrochem. Soc.* **1953**, *100*, 411–419. [[CrossRef](#)]
2. Choi, J. Fabrication of monodomain porous alumina using nano-imprint lithography and its applications. Ph. D. Thesis, Martin-Luther-Universität, Halle-Wittenberg, Germany, 2004.
3. Masuda, H.; Fukuda, K. Ordered metal nanohole arrays made by a two-step replication of honeycomb structures of anodic alumina. *Science* **1995**, *268*, 1466–1468. [[CrossRef](#)] [[PubMed](#)]
4. Masuda, H.; Yamada, H.; Satoh, M.; Asoh, H.; Nakao, M.; Tamamura, T. Highly ordered nanochannel-array architecture in anodic alumina. *Appl. Phys. Lett.* **1997**, *71*, 2770–2772. [[CrossRef](#)]
5. Jessensky, O.; Müller, F.; Gösele, U. Self-organized formation of hexagonal pore arrays in anodic alumina. *Appl. Phys. Lett.* **1998**, *72*, 1173–1175. [[CrossRef](#)]
6. Nakajima, D.; Kikuchi, T.; Natsui, S.; Suzuki, R.O. Highly ordered anodic alumina nanofibers fabricated via two distinct anodizing processes. *ECS Electrochem. Lett.* **2015**, *4*, H14–H17. [[CrossRef](#)]
7. Roy, P.; Berger, S.; Schmuki, P. TiO₂ nanotubes: Synthesis and applications. *Angew. Chem. Int. Ed.* **2011**, *50*, 2904–2939. [[CrossRef](#)] [[PubMed](#)]
8. Lee, K.; Mazare, A.; Schmiki, P. One-dimensional titanium dioxide nanomaterials: Nanotubes. *Chem. Rev.* **2014**, *114*, 9385–9454. [[CrossRef](#)] [[PubMed](#)]

9. Ge, M.-Z.; Cao, C.-Y.; Huang, J.-Y.; Li, S.-H.; Zhang, S.-N.; Deng, S.; Li, Q.-S.; Zhang, K.-Q.; Lai, Y.-K. Synthesis, modification, and photo/photoelectrocatalytic degradation applications of TiO₂ nanotube arrays: A review. *Nanotechnol. Rev.* **2013**, *2*, 27–45. [[CrossRef](#)]
10. Kowalski, D.; Kim, D.; Schmuki, P. TiO₂ nanotubes, nanochannels and mesosponge: Self-organized formation and applications. *Nano Today* **2013**, *8*, 235–264. [[CrossRef](#)]
11. Lee, K. Anodic Growth of Porous Metal Oxides and Their Applications. Ph.D. Thesis, Friedrich-Alexander-Universität, Erangen-Nürnberg, Germany, 2013.
12. Park, J.; Lee, G.; Choi, J. Key anodization factors for determining the formation of TiO₂ microcones vs nanotubes. *J. Electrochem. Soc.* **2017**, *164*, D640–D644. [[CrossRef](#)]
13. Lim, J.H.; Choi, J. Titanium oxide nanowires originated from anodically-grown nanotubes: The bamboo-splitting-model. *Small* **2007**, *3*, 1504–1507. [[CrossRef](#)] [[PubMed](#)]
14. Riboni, F.; Nguyen, N.T.; So, S.; Schmuki, P. Aligned metal oxide nanotube arrays: Key-aspects of anodic TiO₂ nanotube formation and properties. *Nanoscale Horiz.* **2016**, *1*, 445–466. [[CrossRef](#)]
15. Asahi, R.; Morikawa, T.; Ohwaki, T.; Aoki, K.; Taga, Y. Visible-Light Photocatalysis in nitrogen-doped titanium oxides. *Science* **2001**, *293*, 269–271. [[CrossRef](#)] [[PubMed](#)]
16. Schneider, J.; Matuoka, M.; Takeuchi, M.; Zhang, J.; Horiuchi, Y.; Anpo, M.; Bahnemann, D.W. Understanding TiO₂ photocatalysis: Mechanisms and materials. *Chem. Rev.* **2014**, *114*, 9919–9986. [[CrossRef](#)] [[PubMed](#)]
17. Yoo, H.; Choi, Y.-W.; Choi, J. Ruthenium oxide-doped TiO₂ nanotubes by single-step anodization for water-oxidation applications. *ChemCatChem* **2015**, *7*, 643–647. [[CrossRef](#)]
18. Gong, J.; Lai, Y.; Lin, C. Electrochemically multi-anodized TiO₂ nanotube arrays for enhancing hydrogen generation by photoelectrocatalytic water splitting. *Electrochim. Acta* **2010**, *55*, 4776–4782. [[CrossRef](#)]
19. Trasatti, S. Electrocatalysis: Understanding the success of DSA[®]. *Electrochim. Acta* **2000**, *45*, 2377–2385. [[CrossRef](#)]
20. Anantharaj, S.; Ede, S.R.; Sakthikumar, K.; Karkhick, K.; Mishra, S.; Kundu, S. Recent trends and perspectives in electrochemical water splitting with an emphasis on sulfide, selenide, and phosphide catalysts of Fe, Co, and Ni: A review. *ACS Catal.* **2016**, *6*, 8069–8097. [[CrossRef](#)]
21. Matsumoto, Y.; Sato, E. Electrocatalytic properties of transition metal oxides for oxygen eVolution reaction. *Mater. Chem. Phys.* **1986**, *15*, 397–426. [[CrossRef](#)]
22. Bockris, J.O.; Otagawa, T. Mechanism of oxygen eVolution on perovskites. *J. Phys. Chem.* **1983**, *87*, 2960–2971. [[CrossRef](#)]
23. Rungtaweeveranit, B.; Zhao, Y.; Choi, K.M.; Yaghi, O.M. Cooperative effects at the interface of nanocrystalline metal-organic frameworks. *Nano Res.* **2016**, *9*, 47–58. [[CrossRef](#)]
24. Yoo, H.; Oh, K.; Lee, Y.R.; Row, K.H.; Lee, G.; Choi, J. Simultaneous co-doping of RuO₂ and IrO₂ into anodic TiO₂ nanotubes: A binary catalysts for electrochemical water splitting. *Int. J. Hydrogen Energy* **2017**, *42*, 6657–6664. [[CrossRef](#)]
25. Murphy, A.B. Does carbon doping of TiO₂ allow water splitting in visible light? Comments on “Nanotube enhanced photoresponse of carbon modified (CM)-n-TiO₂ for efficient water splitting”. *Sol. Energy Mater. Solar Cells* **2008**, *92*, 363–367. [[CrossRef](#)]
26. Ghicov, A.; Macak, J.M.; Tsuchiya, H.; Kunze, J.; Haeublein, V.; Frey, L.; Schmuki, P. Ion implantation and annealing for an efficient N-doping of TiO₂ nanotubes. *Nano Lett.* **2006**, *6*, 1080–1082. [[CrossRef](#)]
27. Ghicov, A.; Macak, J.M.; Tsuchiya, H.; Kunze, J.; Haeublein, V.; Kleber, S.; Schmuki, P. TiO₂ nanotube layers: Dose effects during nitrogen doping by ion implantation. *Chem. Phys. Lett.* **2006**, *419*, 426–429. [[CrossRef](#)]
28. Macak, J.M.; Ghicov, A.; Hahn, R.; Tsuchiya, H.; Schmuki, P. Photoelectrochemical properties of N-doped self-organized titania nanotube layers with different thicknesses. *J. Mater. Res.* **2006**, *21*, 2824–2828. [[CrossRef](#)]
29. Vitiello, R.P.; Macak, J.M.; Ghicov, A.; Tsuchiya, H.; Dick, L.F.P.; Schmuki, P. N-Doping of anodic TiO₂ nanotubes using heat treatment in ammonia. *Electrochem. Commun.* **2006**, *8*, 544–548. [[CrossRef](#)]
30. Jha, H.; Hahn, R.; Schmuki, P. Ultrafast oxide nanotube formation on TiNb, TiZr and TiTa alloys by rapid breakdown anodization. *Electrochim. Acta* **2010**, *55*, 8883–8887. [[CrossRef](#)]
31. Yoo, H. TiO₂-based electrodes for electrochemical energy conversion and storage. Ph.D. Thesis, Inha University, Incheon, South Korea, August 2018.
32. Gim, Y.; Seong, M.; Choi, Y.-W.; Choi, J. RuO₂-doping into high-aspect-ratio anodic TiO₂ nanotubes by electrochemical potential shock for water oxidation. *Electrochem. Commun.* **2015**, *52*, 37–40. [[CrossRef](#)]

33. Kim, S.; Yoo, H.; Rhee, O.; Choi, J. Doping of Pt into anodic TiO₂ nanotubes for water oxidation: Underpotential shock method in Cl⁻ solution. *J. Phys. Chem. C* **2015**, *119*, 21497–21503. [[CrossRef](#)]
34. Seong, M.; Kim, S.; Yoo, H.; Choi, J. Doping of anodic nanotubular TiO₂ electrodes with MnO₂ for use as catalysts in water oxidation. *Catal. Today* **2016**, *260*, 135–139. [[CrossRef](#)]
35. Albu, S.P.; Tsuchiya, H.; Fujimoto, S.; Schmuki, P. TiO₂ nanotubes—Annealing effects on detailed morphology and structure. *Eur. J. Inorg. Chem.* **2010**, *2010*, 4351–4356. [[CrossRef](#)]
36. Choi, J.; Wehrspohn, R.B.; Lee, J.; Gösele, U. Anodization of nanoimprinted titanium: A comparison with formation of porous alumina. *Electrochim. Acta* **2004**, *49*, 2645–2652. [[CrossRef](#)]
37. Paramasivam, I.; Jha, H.; Liu, N.; Schmuki, P. A review of photocatalysis using self-organized TiO₂ nanotubes and other ordered oxide nanostructures. *Small* **2012**, *8*, 3073–3103. [[CrossRef](#)] [[PubMed](#)]
38. Smith, Y.R.; Ray, R.S.; Carlson, K.; Sarma, B.; Misra, M. Self-ordered titanium dioxide nanotube arrays: Anodic synthesis and their photo/electro-catalytic applications. *Materials* **2013**, *6*, 2892–2957. [[CrossRef](#)] [[PubMed](#)]
39. Altomare, M.; Nguyen, N.T.; Schmuki, P. Templated dewetting: Designing entirely self-organized platforms for photocatalysis. *Chem. Sci.* **2016**, *7*, 6865–6886. [[CrossRef](#)] [[PubMed](#)]
40. Po, C.C.; Chien, C.C.; Shih, H.C. A review on production, characterization, and photocatalytic applications of TiO₂ nanoparticles and nanotubes. *Curr. Nanosci.* **2017**, *13*, 373–393. [[CrossRef](#)]
41. Fu, Y.; Mo, A. A review on the electrochemically self-organized titania nanotube arrays: Synthesis, modifications, and biomedical applications. *Nanoscale Res. Lett.* **2018**, *13*, 187. [[CrossRef](#)] [[PubMed](#)]
42. Awad, N.K.; Edwards, S.L.; Morsi, Y.S. A review of TiO₂ NTs on Ti metal: Electrochemical synthesis, functionalization and potential use as bone implants. *Mater. Sci. Eng. C* **2017**, *76*, 1401–1412. [[CrossRef](#)] [[PubMed](#)]
43. Roy, P.; Kim, D.; Lee, K.; Spiecker, E.; Schmuki, P. TiO₂ nanotubes and their application in dye-sensitized solar cells. *Nanoscale* **2010**, *2*, 45–59. [[CrossRef](#)] [[PubMed](#)]
44. Kim, S.; Seong, M.; Choi, J. Rapid breakdown anodization for the preparation of titania nanotubes in halogen-free acid. *J. Electrochem. Soc.* **2015**, *162*, C205–C208. [[CrossRef](#)]
45. Hahn, R.; Macák, J.M.; Schmuki, P. Rapid anodic growth of TiO₂ and WO₃ nanotubes in fluoride free electrolytes. *Electrochem. Commun.* **2007**, *9*, 947–957. [[CrossRef](#)]
46. Nguyen, Q.A.; Bhargava, Y.V.; Devine, T.M. Titania nanotube formation in chloride and bromide containing electrolytes. *Electrochem. Commun.* **2008**, *10*, 471–475. [[CrossRef](#)]
47. Yoo, H.; Oh, K.; Nah, Y.-C.; Choi, J.; Lee, K. Single-step anodization for formation of WO₃-doped TiO₂ nanotubes toward enhanced electrochromic performance. *ChemElectroChem* **2018**, *5*, 3379–3382. [[CrossRef](#)]
48. Macák, J.M.; Tsuchiyam, H.; Schmuki, P. High-aspect-ratio TiO₂ nanotubes by anodization of titanium. *Angew. Chem. Int. Ed.* **2005**, *44*, 2100–2102. [[CrossRef](#)] [[PubMed](#)]
49. Lee, B.G.; Nam, S.-C.; Choi, J. Anodic TiO₂ nanotubes as anode electrode in Li-air and Li-ion batteries. *Curr. Appl. Phys.* **2012**, *12*, 1580–1585. [[CrossRef](#)]
50. Paulose, M.; Shankar, K.; Yoriya, S.; Prakasam, H.E.; Varghese, O.K.; Mor, G.K.; Latempa, T.A.; Fitzgerald, A.; Grimes, C.A. Anodic growth of highly ordered TiO₂ nanotube arrays to 134 μm in length. *J. Phys. Chem. B* **2006**, *110*, 16179–16184. [[CrossRef](#)] [[PubMed](#)]
51. Shankar, K.; Mor, G.; Fitzgerald, K.A.; Grimes, C.A. Cation effect on the electrochemical formation of very high aspect ratio TiO₂ nanotube arrays in formamide–water mixtures. *J. Phys. Chem. C* **2007**, *111*, 21–26. [[CrossRef](#)]
52. Yin, H.; Liu, H.; Shen, W.Z. The large diameter and fast growth of self-organized TiO₂ nanotube arrays achieved via electrochemical anodization. *Nanotechnol.* **2010**, *21*, 035601. [[CrossRef](#)] [[PubMed](#)]
53. Elzarka, A.; Liu, N.; Hwang, I.; Kamal, M.; Schmuki, P. Large-diameter TiO₂ nanotubes enable wall engineering with conformal hierarchical decoration and blocking layers for enhanced efficiency in dye-sensitized solar cells (DSSC). *Chem. Eur. J.* **2017**, *23*, 12995–12999. [[CrossRef](#)] [[PubMed](#)]
54. Lee, K.; Schmuki, P. Bottom sealing and photoelectrochemical properties of different types of anodic TiO₂ nanotubes. *Electrochim. Acta* **2013**, *100*, 229–235. [[CrossRef](#)]
55. Chen, X.; Schriver, M.; Suen, T.; Mao, S.S. Fabrication of 10 nm diameter TiO₂ nanotube arrays by titanium anodization. *Thin Solid Films* **2007**, *515*, 8511–8514. [[CrossRef](#)]

56. Hoseinzadeh, T.; Ghorannevis, Z.; Ghoranneviss, M.; Sari, A.H.; Salem, M.K. Effects of various applied voltages on physical properties of TiO₂ nanotubes by anodization method. *J. Theor. Appl. Phys.* **2017**, *11*, 243–248. [[CrossRef](#)]
57. Atyaoui, A.; Cachet, H.; Sutter, E.M.M.; Bousselmi, L. Effect of the anodization voltage on the dimensions and photoactivity of titania nanotubes arrays. *Surf. Interface Anal.* **2013**, *45*, 1751–1759. [[CrossRef](#)]
58. Cha, G.; Lee, H.J.; Choi, J. Preparation of binder-free thin film Li₄Ti₅O₁₂ anode with an adjustable thickness through anodic TiO₂ nanotubes. *Curr. Appl. Phys.* **2013**, *13*, 1788–1795. [[CrossRef](#)]
59. Kim, D.; Ghicov, A.; Schmuki, P. TiO₂ Nanotube arrays: Elimination of disordered top layers (“nanograss”) for improved photoconversion efficiency in dye-sensitized solar cells. *Electrochem. Commun.* **2008**, *10*, 1835–1838. [[CrossRef](#)]
60. Ma, X.; Sun, Z.; Hu, X. Synthesis of tin and molybdenum co-doped TiO₂ nanotube arrays for the photoelectrocatalytic oxidation of phenol in aqueous solution. *Mater. Sci. Semicond. Proc.* **2018**, *85*, 150–159. [[CrossRef](#)]
61. Jo, Y.; Jung, I.; Lee, I.; Choi, J.; Tak, Y. Fabrication of through-hole TiO₂ nanotubes by potential shock. *Electrochem. Comm.* **2010**, *12*, 616–619. [[CrossRef](#)]
62. Shin, S.; Kim, K.; Choi, J. Fabrication of ruthenium-doped TiO₂ electrodes by one-step anodization for electrolysis applications. *Electrochem. Commun.* **2013**, *36*, 88–91. [[CrossRef](#)]
63. Shin, S.; Choi, Y.-W.; Choi, J. Water splitting by dimensionally stable anode prepared through micro-arc oxidation. *Mater. Lett.* **2013**, *105*, 117–119. [[CrossRef](#)]
64. Wei, W.; Oltean, G.; Tai, C.-W.; Edström, K.; Björefors, F.; Nyholm, L. High energy and power density TiO₂ nanotube electrodes for 3D Li-ion microbatteries. *J. Mater. Chem. A* **2013**, *1*, 8160–8170. [[CrossRef](#)]
65. Sitler, S.J.; Raja, K.S.; Karmiol, Z.; Chidambaram, D. Photoelectrochemical characterization of dual-layered anodic TiO₂ nanotubes with honeycomb morphology. *J. Phys. D Appl. Phys.* **2016**, *50*, 035502. [[CrossRef](#)]
66. Wang, X.; Zhang, S.; Sun, L. A Two-step anodization to grow high-aspect-ratio TiO₂ nanotubes. *Thin Solid Films* **2011**, *519*, 4694–4698. [[CrossRef](#)]
67. Albu, S.P.; Ghicov, A.; Aldabergenova, S.; Drechsel, P.; LeClere, D.; Thompson, G.E.; Macak, J.M.; Schmuki, P. Formation of double-walled TiO₂ nanotubes and robust anatase membranes. *Adv. Mater.* **2008**, *20*, 4135–4139. [[CrossRef](#)]
68. Beranek, R.; Tsuchiya, H.; Sugishima, T.; Macak, J.M.; Taveira, L.; Fujimoto, S.; Kisch, H.; Schmuki, P. Enhancement and limits of the photoelectrochemical response from anodic TiO₂ nanotubes. *Appl. Phys. Lett.* **2005**, *87*, 243114. [[CrossRef](#)]
69. Beranek, R.; Hildebrand, H.; Schmuki, P. Self-organized porous titanium oxide prepared in H₂SO₄/HF electrolytes. *Electrochem. Sol. State Lett.* **2003**, *6*, B12–B14. [[CrossRef](#)]
70. Wang, H.; Lewis, J.P. Second-generation photocatalytic materials: Anion-doped TiO₂. *J. Phys. Condens. Matter.* **2006**, *18*, 421–434. [[CrossRef](#)]
71. Irie, H.; Watanabe, Y.; Hashimoto, K. Nitrogen-concentration dependence on photocatalytic activity of TiO_{2-x}N_x powders. *J. Phys. Chem. B* **2003**, *107*, 5483–5486. [[CrossRef](#)]
72. Zhao, Z.; Liu, Q. Mechanism of higher photocatalytic activity of anatase TiO₂ doped with nitrogen under visible-light irradiation from density functional theory calculation. *J. Phys. D Appl. Phys.* **2008**, *41*, 025105. [[CrossRef](#)]
73. Qiu, X.; Burda, C. Chemically synthesized nitrogen-doped metal oxide nanoparticles. *Chem. Phys. Lett.* **2007**, *339*, 1–10. [[CrossRef](#)]
74. Prokes, S.M.; Gole, J.L.; Chen, X.; Burda, C.; Carlos, W.E. Defect-related optical behavior in surface modified TiO₂ nanostructures. *Adv. Funct. Mater.* **2005**, *15*, 161–167. [[CrossRef](#)]
75. Liu, S.; Yang, L.; Xu, S.; Luo, S.; Cai, Q. Photocatalytic activities of C–N-doped TiO₂ nanotube array/carbon nanorod composite. *Electrochem. Commun.* **2009**, *11*, 1748–1751. [[CrossRef](#)]
76. Beranek, R.; Macak, J.M.; Gartner, M.; Meyer, K.; Schmuki, P. Enhanced visible light photocurrent generation at surface-modified TiO₂ nanotubes. *Electrochim. Acta* **2009**, *54*, 2640–2646. [[CrossRef](#)]
77. Mazare, A.; Paramasivam, I.; Schmidt-Stein, F.; Lee, K.; Demetrescu, I.; Schmuki, P. Flame annealing effects on self-organized TiO₂ nanotubes. *Electrochim. Acta* **2012**, *66*, 12–21. [[CrossRef](#)]
78. Yang, K.; Dai, Y.; Huang, B.; Whangbo, M.-H. Density functional characterization of the visible-light absorption in substitutional C-anion- and C-cation-doped TiO₂. *J. Phys. Chem. C* **2009**, *1*, 2624–2629. [[CrossRef](#)]

79. Park, J.H.; Kim, S.; Bard, A.J. Novel carbon-doped TiO₂ nanotube arrays with high aspect ratios for efficient solar water splitting. *Nano Lett.* **2006**, *6*, 24–28. [[CrossRef](#)] [[PubMed](#)]
80. Hahn, R.; Ghicov, A.; Salonen, J.; Lehto, V.-P.; Schmuki, P. Carbon doping of self-organized TiO₂ nanotube layers by thermal acetylene treatment. *Nanotechnology* **2007**, *18*, 105604. [[CrossRef](#)]
81. Barborini, E.; Conti, A.M.; Kholmanov, I.; Piseri, P.; Podesta, A.; Milani, P.; Cepek, C.; Sakho, O.; Macovez, R.; Sancrotti, M. Nanostructured TiO₂ films with 2 eV optical gap. *Adv. Mater.* **2005**, *17*, 1842–1846. [[CrossRef](#)]
82. Yang, L.; Luo, S.; Liu, S.; Cai, Q. Graphitized carbon nanotubes formed in TiO₂ nanotube arrays: A novel functional material with tube-in-tube nanostructure. *J. Phys. Chem. C* **2008**, *112*, 8939–8943. [[CrossRef](#)]
83. Hahn, R.; Schmidt-Stein, F.; Salonen, J.; Thiemann, S.; Song, Y.Y.; Kunze, J.; Lehto, V.-P.; Schmuki, P. Semimetallic TiO₂ nanotubes. *Angew. Chem. Int. Ed.* **2009**, *48*, 7236–7239. [[CrossRef](#)] [[PubMed](#)]
84. Song, Y.-Y.; Roy, P.; Paramasivam, I.; Schmuki, P. Voltage-induced payload release and wettability control on TiO₂ and TiO₂ nanotubes. *Angew. Chem. Int. Ed.* **2010**, *49*, 351–354. [[CrossRef](#)] [[PubMed](#)]
85. Aruna, S.T.; Tirosh, S.; Zaban, A. Nanosize rutile titania particle synthesis via a hydrothermal method without mineralizers. *J. Mater. Chem.* **2000**, *10*, 2388–2391. [[CrossRef](#)]
86. Kim, D.; Tsuchiya, H.; Fujimoto, S.; Schmidt-Stein, F.; Schmuki, P. Nitrogen-doped TiO₂ mesosponge layers formed by anodization of nitrogen-containing Ti alloys. *J. Solid State Electrochem.* **2012**, *16*, 89–92. [[CrossRef](#)]
87. Nah, Y.-C.; Ghicov, A.; Kim, D.; Berger, S.; Schmuki, P. TiO₂–WO₃ Composite nanotubes by alloy anodization: Growth and enhanced electrochromic properties. *J. Am. Chem. Soc.* **2008**, *130*, 16154–16155. [[CrossRef](#)] [[PubMed](#)]
88. Ghicov, A.; Yamamoto, M.; Schmuki, P. Lattice Widening in niobium-doped TiO₂ nanotubes: Efficient ion intercalation and swift electrochromic contrast. *Angew. Chem. Int. Ed.* **2008**, *47*, 7934–7937. [[CrossRef](#)] [[PubMed](#)]
89. Agarwal, P.; Paramasivam, I.; Shrestha, N.K.; Schmuki, P. MoO₃ in Self-organized TiO₂ nanotubes for enhanced photocatalytic activity. *Chem. Asian J.* **2010**, *5*, 66–69. [[CrossRef](#)] [[PubMed](#)]
90. Czoska, A.; Livraghi, S.; Chiesa, M.; Giamello, E.; Agnoli, S.; Granozzi, S.; Finazzi, E.; Valentin, C.D.; Pacchioni, G. The nature of defects in fluorine-doped TiO₂. *J. Phys. Chem. C* **2008**, *112*, 8951–8956. [[CrossRef](#)]
91. Osorio-Guillen, J.; Lany, S.; Zunger, A. Atomic control of conductivity versus ferromagnetism in wide-gap oxides via selective doping: V, Nb, Ta in anatase TiO₂. *Phys. Rev. Lett.* **2008**, *100*, 036601. [[CrossRef](#)] [[PubMed](#)]
92. Wang, Y.; Doren, D. Electronic structures of V-doped anatase TiO₂. *Solid State Commun.* **2005**, *136*, 142–146. [[CrossRef](#)]
93. Valentin, C.D.; Pacchioni, G.; Onishi, H.; Kudo, A. Cr/Sb co-doped TiO₂ from first principles calculations. *Chem. Phys. Lett.* **2009**, *469*, 166–171. [[CrossRef](#)]
94. Shao, G.J. Red shift in manganese- and iron-doped TiO₂: A DFT+U analysis. *Phys. Chem. C* **2009**, *113*, 6800–6808. [[CrossRef](#)]
95. Hotsenpiller, P.A.M.; Bolt, J.D.; Farneth, W.E.; Lowekamp, J.B.; Rohrer, G.S. Orientation dependence of photochemical reactions on TiO₂ surfaces. *J. Phys. Chem. B* **1998**, *102*, 3216–3226. [[CrossRef](#)]
96. Casarin, M.; Maccato, C.; Vittadini, A. Electronic structure of Nb impurities in and on TiO₂. *Phys. Chem. Chem. Phys.* **1999**, *1*, 3793–3799. [[CrossRef](#)]
97. Atashbar, M.Z.; Sun, H.T.; Gong, B.; Wlodarski, W.; Lamb, R. XPS study of Nb-doped oxygen sensing TiO₂ thin films prepared by sol-gel method. *Thin Solid Films* **1998**, *326*, 238–244. [[CrossRef](#)]
98. Stodolny, M.; Laniecki, M. Synthesis and characterization of mesoporous Ta₂O₅–TiO₂ photocatalysts for water splitting. *Catal. Today* **2009**, *142*, 314–319. [[CrossRef](#)]
99. Fernandez-Garcia, M.; Martinez-Arias, A.; Fuente, A.; Conesa, J.C. Nanostructured Ti–W mixed-metal oxides: Structural and electronic properties. *J. Phys. Chem. B* **2005**, *109*, 6075–6083. [[CrossRef](#)] [[PubMed](#)]
100. Tsuchiya, H.; Macak, J.M.; Ghicov, A.; Schmuki, P. Self-organization of anodic nanotubes on two size scales. *Small* **2006**, *2*, 888–891. [[CrossRef](#)] [[PubMed](#)]
101. Tsuchiya, H.; Akaki, T.; Terada, D.; Tsuji, N.; Minamino, Y.; Schmuki, P.; Fujimoto, S. Metallurgical aspects on the formation of self-organized anodic oxide nanotube layers. *Electrochim. Acta* **2009**, *54*, 5155–5162. [[CrossRef](#)]
102. Macak, J.M.; Tsuchiya, H.; Ghicov, A.; Yasuda, K.; Hahn, R.; Bauer, S.; Schmuki, P. TiO₂ nanotubes: Self-organized electrochemical formation, properties and applications. *Curr. Opin. Solid State Mater. Sci.* **2007**, *11*, 3–18. [[CrossRef](#)]

103. Tsuchiya, H.; Akaki, T.; Nakata, J.; Terada, D.; Tsuji, N.; Koizumi, Y.; Minamino, Y.; Schmuki, P.; Fujimoto, S. Anodic oxide nanotube layers on Ti–Ta alloys: Substrate composition, microstructure and self-organization on two-size scales. *Corros. Sci.* **2009**, *51*, 1528–1533. [[CrossRef](#)]
104. Feng, X.J.; Macak, J.M.; Albu, S.P.; Schmuki, P. Electrochemical formation of self-organized anodic nanotube coating on Ti–28Zr–8Nb biomedical alloy surface. *Acta Biomater.* **2008**, *4*, 318–323. [[CrossRef](#)] [[PubMed](#)]
105. Yasuda, K.; Schmuki, P. Control of morphology and composition of self-organized zirconium titanate nanotubes formed in (NH₄)₂SO₄/NH₄F electrolytes. *Electrochim. Acta* **2007**, *52*, 4053–4061. [[CrossRef](#)]
106. Yasuda, K.; Macak, J.M.; Berger, S.; Ghicov, A.; Schmuki, P. Mechanistic aspects of the self-organization process for oxide nanotube formation on valve metals. *J. Electrochem. Soc.* **2007**, *154*, C472–C478. [[CrossRef](#)]
107. Yasuda, K.; Schmuki, P. Electrochemical formation of self-organized zirconium titanate nanotube multilayers. *Electrochem. Commun.* **2007**, *9*, 615–619. [[CrossRef](#)]
108. Kamkin, A.N.; Fishgoit, L.A.; Davydov, A.D. Composition and structure of anodic oxide films on titanium–aluminum alloys by fast electron reflection diffraction, rutherford backscattering, and secondary neutral particle mass spectrometry. *Russ. J. Electrochem.* **2003**, *39*, 665–670. [[CrossRef](#)]
109. Yasuda, K.; Schmuki, P. Formation of self-organized zirconium titanate nanotube layers by alloy anodization. *Adv. Mater.* **2007**, *19*, 1757–1760. [[CrossRef](#)]
110. Nah, Y.C.; Ghicov, A.; Kim, D.; Schmuki, P. Enhanced electrochromic properties of self-organized nanoporous WO₃. *Electrochem. Commun.* **2008**, *10*, 1777–1780. [[CrossRef](#)]
111. Shrestha, N.K.; Nah, Y.C.; Tsuchiya, H.; Schmuki, P. Self-organized nano-tubes of TiO₂–MoO₃ with enhanced electrochromic properties. *Chem. Commun.* **2009**, *15*, 2008–2010. [[CrossRef](#)] [[PubMed](#)]
112. Benoit, A.; Paramasivam, I.; Nah, Y.C.; Roy, P.; Schmuki, P. Decoration of TiO₂ nanotube layers with WO₃ nanocrystals for high-electrochromic activity. *Electrochem. Commun.* **2009**, *11*, 728–732. [[CrossRef](#)]
113. Yang, M.; Shrestha, N.K.; Schmuki, P. Thick porous tungsten trioxide films by anodization of tungsten in fluoride containing phosphoric acid electrolyte. *Electrochem. Commun.* **2009**, *11*, 1908–1911. [[CrossRef](#)]
114. So, S.; Lee, K.; Schmuki, P. Ru-doped TiO₂ nanotubes: Improved performance in dye-sensitized solar cells. *Phys. Status Solidi RRL* **2012**, *6*, 169–171. [[CrossRef](#)]
115. Doyle, R.L.; Lyons, M.E.G. *The Oxygen eVolution Reaction: Mechanistic Concepts and Catalyst Design*; Giménez, S., Bisquert, J., Eds.; Photoelectrochemical Solar Fuel Production; Springer: Cham, Switzerland, 2016.
116. Suen, N.-T.; Hung, S.-F.; Quan, Q.; Zhang, N.; Xu, Y.-J.; Chen, H.M. Electrocatalysis for the oxygen eVolution reaction: Recent development and future perspectives. *Chem. Soc. Rev.* **2017**, *46*, 337–365. [[CrossRef](#)] [[PubMed](#)]
117. Reier, T.; Nong, H.N.; Teschner, D.; Schlögl, R.; Strasser, P. Electrocatalytic oxygen eVolution reaction in acidic environments—Reaction mechanisms and catalysts. *Adv. Energy Mater.* **2017**, *7*, 1601275–1601293. [[CrossRef](#)]
118. Matyushcov, V. Standard electrode potential, Tafel equation, and the solvation thermodynamics. *J. Chem. Phys.* **2009**, *130*, 234704–234804. [[CrossRef](#)] [[PubMed](#)]
119. Trasatti, S. Electrocatalysis in the anodic eVolution of oxygen and chlorine. *Electrochim. Acta* **1984**, *29*, 1503–1512. [[CrossRef](#)]
120. Castelli, P.; Trasatti, S.; Pollak, F.H.; Ogrady, W.E. Single crystals as model electrocatalysts: Oxygen eVolution on RuO₂ (110). *J. Electroanal. Chem.* **1986**, *210*, 189–194. [[CrossRef](#)]
121. Yoo, H.; Oh, K.; Lee, G.; Choi, J. RuO₂-doped Anodic TiO₂ nanotubes for water oxidation: Single-step anodization vs potential shock method. *J. Electrochem. Soc.* **2017**, *164*, H104–H111. [[CrossRef](#)]
122. Bockris, J.O.; Nagy, Z. Symmetry factor and Transfer coefficient; A source of confusion in electrode kinetics. *J. Chem. Edu.* **1973**, *50*, 839–843. [[CrossRef](#)]
123. Conway, B.E.; Salomon, M. Electrochemical reaction orders: Applications to the hydrogen- and oxygen-evolution reactions. *Electrochim. Acta* **1964**, *9*, 1599–1615. [[CrossRef](#)]
124. Conway, B.E.; Bai, L.; Sattar, M.A. Role of the transfer coefficient in electrocatalysis: Applications to the H₂ and O₂ eVolution reactions and the characterization of participating adsorbed intermediates. *Int. J. Hydrogen Energy* **1987**, *12*, 607–621. [[CrossRef](#)]
125. Rossmeisl, J.; Logadottir, A.; Nørskov, J.K. Electrolysis of water on (oxidized) metal surfaces. *Chem. Phys.* **2005**, *319*, 178–184. [[CrossRef](#)]

126. Medford, A.J.; Voivodic, A.; Hummelshøj, J.S.; Voss, J.; Abild-Pedersen, F.; Studt, F.; Bligaard, T.; Nilsson, A.; Nørskov, J.K. From the Sabatier principle to a predictive theory of transition-metal heterogeneous catalysis. *J. Catal.* **2015**, *328*, 36–42. [[CrossRef](#)]
127. Fabbri, E.; Havereder, A.; Waltar, K.; Kötz, R.; Schmidt, T.J. Developments and perspectives of oxide-based catalysts for the oxygen eVolution reaction. *Catal. Sci. Technol.* **2014**, *4*, 3800–3821. [[CrossRef](#)]
128. Kötz, R.; Stucki, S. Stabilization of RuO₂ by IrO₂ for anodic oxygen eVolution in acid media. *Electrochim. Acta* **1986**, *31*, 1311–1316. [[CrossRef](#)]
129. Yeo, R.S.; Orehtsky, J.; Visscher, W.; Srinivasan, S. Ruthenium-based mixed oxides as electrocatalysts for oxygen eVolution in acid electrolytes. *J. Electrochem. Soc.* **1981**, *128*, 1900–1904. [[CrossRef](#)]
130. Fujishima, A.; Honda, K. Electrochemical photolysis of water at a semiconductor electrode. *Nature* **1972**, *238*, 37–38. [[CrossRef](#)] [[PubMed](#)]
131. Fujishima, A.; Zhang, X.; Tryk, D.A. TiO₂ photocatalysis and related surface phenomena. *Surf. Sci. Rep.* **2008**, *63*, 515–582. [[CrossRef](#)]
132. Masudy-Panah, S.; Eugene, Y.-J.K.; Khiavi, N.D.; Katal, R.; Gong, X. Aluminum-incorporated p-CuO/n-ZnO photocathode coated with nanocrystal-engineered TiO₂ protective layer for photoelectrochemical water splitting and hydrogen generation. *J. Mater. Chem. A* **2018**, *6*, 11951–11965. [[CrossRef](#)]
133. Katal, R.; Panah, S.M.; Zarinejad, M.; Salehi, M.; Jiangyong, H. Synthesis of self-gravity settling faceted-anatase TiO₂ with dominant {010} facets for the photocatalytic degradation of acetaminophen and study of the type of generated oxygen vacancy in faceted-TiO₂. *Water* **2018**, *10*, 1462. [[CrossRef](#)]
134. Katal, R.; Salehi, M.; Farahani, M.H.D.A.; Masudy-Panah, S.; Ong, S.L.; Hu, J. Preparation of a new type of black TiO₂ under a vacuum atmosphere for sunlight photocatalysis. *ACS Appl. Mater. Interfaces* **2018**, *10*, 35316–35326. [[CrossRef](#)] [[PubMed](#)]
135. Moakhar, R.S.; Masudy-Panah, S.; Jalali, M.; Goh, G.K.L.; Dolati, A.; Ghorbani, M.; Riahi-Noori, N. Sunlight driven photoelectrochemical light-to-electricity conversion of screen-printed surface nanostructured TiO₂ decorated with plasmonic Au nanoparticles. *Electrochim. Acta* **2016**, *219*, 386–393. [[CrossRef](#)]
136. Ghosh, M.; Liu, J.; Chuang, S.S.C.; Jana, S.C. Fabrication of hierarchical V₂O₅ nanorods on TiO₂ nanofibers and their enhanced photocatalytic activity under visible light. *ChemCatChem* **2018**, *10*, 3305–3318. [[CrossRef](#)]
137. Paramasivam, I.; Macak, J.M.; Schmuki, P. Photocatalytic activity of TiO₂ nanotube layers loaded with Ag and Au nanoparticles. *Electrochem. Commun.* **2008**, *10*, 71–75. [[CrossRef](#)]
138. Macak, J.M.; Zlamal, M.; Krysa, J.; Schmuki, P. Self-organized TiO₂ nanotube layers as highly efficient photocatalysts. *Small* **2007**, *3*, 300–304. [[CrossRef](#)] [[PubMed](#)]
139. Sohn, Y.S.; Smith, Y.R.; Misra, M.; Subramanian, V. Electrochemically assisted photocatalytic degradation of methyl orange using anodized titanium dioxide nanotubes. *Appl. Catal. B Environ.* **2008**, *84*, 372–378. [[CrossRef](#)]
140. Wang, D.; Liu, L.; Zhang, F.; Tao, K.; Pippel, E.; Domen, K. Spontaneous phase and morphology transformations of anodized titania nanotubes induced by water at room temperature. *Nano Lett.* **2011**, *11*, 3649–3655. [[CrossRef](#)] [[PubMed](#)]
141. Paramasivam, I.; Nah, Y.-C.; Das, C.; Shrestha, N.K.; Schmuki, P. WO₃/TiO₂ nanotubes with strongly enhanced photocatalytic activity. *Chem. Eur. J.* **2010**, *16*, 8993–8997. [[CrossRef](#)] [[PubMed](#)]
142. Mohapatra, S.K.; Misra, M.; Mahajan, V.K.; Raja, K.S. A novel method for the synthesis of titania nanotubes using sonoelectrochemical method and its application for photoelectrochemical splitting of water. *J. Catal.* **2007**, *246*, 362–369. [[CrossRef](#)]
143. Allam, N.K.; Shankar, K.; Grimes, C.A. Photoelectrochemical and water photoelectrolysis properties of ordered TiO₂ nanotubes fabricated by Ti anodization in fluoride-free HCl electrolytes. *J. Mater. Chem.* **2008**, *18*, 2341–2348. [[CrossRef](#)]
144. Mohapatra, S.K.; Misra, M.; Mahajan, V.K.; Raja, K.S. Design of a highly efficient photoelectrolytic cell for hydrogen generation by water splitting: Application of TiO_{2-x}C_x nanotubes as a photoanode and Pt/TiO₂ nanotubes as a cathode. *J. Phys. Chem. C* **2007**, *111*, 8677–8685. [[CrossRef](#)]
145. Mahajan, V.K.; Misra, M.; Raja, K.S.; Mohapatra, S.K. Self-organized TiO₂ nanotubular arrays for photoelectrochemical hydrogen generation: Effect of crystallization and defect structure. *J. Phys. D Appl. Phys.* **2008**, *41*, 125307. [[CrossRef](#)]
146. Nam, W.; Han, G.Y. Preparation and characterization of anodized Pt-TiO₂ nanotube arrays for water splitting. *J. Chem. Eng. Jpn.* **2007**, *40*, 266–269. [[CrossRef](#)]

147. Ghicov, A.; Schmidt, B.; Kunze, J.; Schmuki, P. Photoresponse in the visible range from Cr doped TiO₂ nanotubes. *Chem. Phys. Lett.* **2007**, *433*, 323–326. [[CrossRef](#)]
148. Das, C.; Roy, P.; Yang, M.; Jha, H.; Schmuki, P. Nb doped TiO₂ nanotubes for enhanced photoelectrochemical water-splitting. *Nanoscale* **2011**, *3*, 3094–3096. [[CrossRef](#)] [[PubMed](#)]
149. Roy, P.; Das, C.; Lee, K.; Hahn, R.; Ruff, T.; Moll, M.; Schmuki, P. Oxide nanotubes on Ti–Ru alloys: Strongly enhanced and stable photoelectrochemical activity for water splitting. *J. Am. Chem. Soc.* **2011**, *133*, 5629–5631. [[CrossRef](#)] [[PubMed](#)]
150. Yang, M.; Jha, H.; Liu, N.; Schmuki, P. Increased photocurrent response in Nb-doped TiO₂ nanotubes. *J. Mater. Chem.* **2011**, *21*, 15205–15208. [[CrossRef](#)]
151. Altomare, M.; Lee, K.; Killian, M.S.; Selli, E.; Schmuki, P. Ta-Doped TiO₂ nanotubes for enhanced solar-light photoelectrochemical water splitting. *Chem. Eur. J.* **2013**, *19*, 5841–5844. [[CrossRef](#)] [[PubMed](#)]
152. Kawai, T.; Sakata, T. Conversion of carbohydrate into hydrogen fuel by a photocatalytic process. *Nature* **1980**, *286*, 474–476. [[CrossRef](#)]
153. Sakata, T.; Hashimoto, K.; Kawai, T. Catalytic properties of ruthenium oxide on n-type semiconductors under illumination. *J. Phys. Chem.* **1984**, *88*, 5214–5221. [[CrossRef](#)]
154. Blondeel, G.; Harriman, A.; Porter, G.; Urwin, D.; Kiwi, J. Design, preparation and characterization of ruthenium dioxide/titanium dioxide catalytic surfaces active in photooxidation of water. *J. Phys. Chem.* **1983**, *87*, 2629–2636. [[CrossRef](#)]
155. O'Regan, B.; Grätzel, M. A low-cost, high-efficiency solar cell based on dye-sensitized colloidal TiO₂ films. *Nature* **1991**, *353*, 737–740. [[CrossRef](#)]
156. Grätzel, M. Photoelectrochemical cells. *Nature* **2001**, *414*, 338–344. [[CrossRef](#)] [[PubMed](#)]
157. Nazeeruddin, M.K.; Angelis, F.D.; Fantacci, S.; Selloni, A.; Viscardi, G.; Liska, P.; Ito, S.; Takeru, B.; Grätzel, M. Combined experimental and DFT-TDDFT computational study of photoelectrochemical cell ruthenium sensitizers. *J. Am. Chem. Soc.* **2005**, *127*, 16835–16847. [[CrossRef](#)] [[PubMed](#)]
158. Tachibana, Y.; Moser, J.E.; Grätzel, M.; Klug, D.R.; Durrant, J.R. Subpicosecond interfacial charge separation in dye-sensitized nanocrystalline titanium dioxide films. *J. Phys. Chem.* **1996**, *100*, 20056–20062. [[CrossRef](#)]
159. Peter, L.M. Characterization and modeling of dye-sensitized solar cells. *J. Phys. Chem. C* **2007**, *111*, 6601–6612. [[CrossRef](#)]
160. Bailes, M.; Cameron, P.J.; Lobato, K.; Peter, L.M. Determination of the density and energetic distribution of electron traps in dye-sensitized nanocrystalline solar cells. *J. Phys. Chem. B* **2005**, *109*, 15429–15435. [[CrossRef](#)] [[PubMed](#)]
161. Cameron, P.J.; Peter, L.M. How does back-reaction at the conducting glass substrate influence the dynamic photovoltage response of nanocrystalline dye-sensitized solar cells? *J. Phys. Chem. B* **2005**, *109*, 7392–7398. [[CrossRef](#)] [[PubMed](#)]
162. Jennings, J.R.; Peter, L.M. A Reappraisal of the electron diffusion length in solid-state dye-sensitized solar cells. *J. Phys. Chem. C* **2007**, *111*, 16100–16104. [[CrossRef](#)]
163. Fujihara, K.; Kumar, A.; Jose, R.; Ramakrishna, S.; Uchida, S. Spray deposition of electrospun TiO₂ nanorods for dye-sensitized solar cell. *Nanotechnology* **2007**, *18*, 365709. [[CrossRef](#)]
164. Zhu, K.; Vinzant, T.B.; Neale, N.R.; Frank, A.J. Removing structural disorder from oriented tio₂ nanotube arrays: Reducing the dimensionality of transport and recombination in dye-sensitized solar cells. *Nano Lett.* **2007**, *7*, 3739–3746. [[CrossRef](#)] [[PubMed](#)]
165. Zhu, K.; Neale, N.R.; Miedaner, A.; Frank, A.J. Enhanced charge-collection efficiencies and light scattering in dye-sensitized solar cells using oriented TiO₂ nanotubes arrays. *Nano Lett.* **2007**, *7*, 69–74. [[CrossRef](#)] [[PubMed](#)]
166. Jennings, J.R.; Ghicov, A.; Peter, L.M.; Schmuki, P.; Walker, A.B. Dye-sensitized solar cells based on oriented TiO₂ nanotube arrays: Transport, trapping, and transfer of electrons. *J. Am. Chem. Soc.* **2008**, *130*, 13364–13372. [[CrossRef](#)] [[PubMed](#)]
167. Zhang, W.; Xie, Y.; Xiong, D.; Zeng, X.; Li, Z.; Wang, M.; Cheng, Y.-B.; Chen, W.; Yang, K.; Yang, S. TiO₂ nanorods: A facile size- and shape-tunable synthesis and effective improvement of charge collection kinetics for dye-sensitized solar cells. *ACS Appl. Mater. Interfaces* **2014**, *6*, 9698–9704. [[CrossRef](#)] [[PubMed](#)]

168. Yang, M.; Kim, D.; Jha, H.; Lee, K.; Paul, J.; Schmuki, P. Nb doping of TiO₂ nanotubes for an enhanced efficiency of dye-sensitized solar cells. *Chem. Commun.* **2011**, *47*, 2032–2034. [[CrossRef](#)] [[PubMed](#)]
169. Lee, K.; Schmuki, P. Ta doping for an enhanced efficiency of TiO₂ nanotube based dye-sensitized solar cells. *Electrochem. Commun.* **2012**, *25*, 11–14. [[CrossRef](#)]



© 2018 by the authors. Licensee MDPI, Basel, Switzerland. This article is an open access article distributed under the terms and conditions of the Creative Commons Attribution (CC BY) license (<http://creativecommons.org/licenses/by/4.0/>).